Generalized Waveform Design for Sidelobe Reduction in MIMO Radar Systems

Ehsan Raei, *Member, EURASIP,*
Mohammad Alaee-Kerahroodi, *Member, EURASIP,*
Prabhu Babu, and M.R. Bhavani Shankar, *Member, EURASIP*

Abstract

Multiple-input multiple-output (MIMO) radars transmit a set of sequences that exhibit small cross-correlation sidelobes, which enhance sensing performance by separating them at the matched filter outputs. Small auto-correlation sidelobes are also required in order to avoid masking of weak targets by the range sidelobes of strong targets and to mitigate the negative effects of distributed clutter. In light of these requirements, in this paper, we design a set of phase-only (constant modulus) sequences that exhibit near-optimal properties in terms of Peak Sidelobe Level (PSL) and Integrated Sidelobe Level (ISL). At the design stage, we adopt weighted ℓ_p-norm of auto- and cross-correlation sidelobes as the objective function and minimize it for a general p value, using block successive upper bound minimization (BSUM). Considering the limitation of radar amplifiers, we design unimodular sequences which make the design problem non-convex and NP-hard. To tackle the problem, in every iteration of the BSUM algorithm, we introduce different local approximation functions and optimize them concerning a block, containing a code entry or a code vector. The numerical results show that the performance of the optimized set of sequences outperforms the state-of-the-art counterparts, in terms of both PSL values and computational time.

Index Terms – BSUM, ℓ_p-norm, PSL, ISL, MIMO Radar, Waveform Design.

I. Introduction

A complex problem in radar pulse compression (intra-pulse modulation) is the design of waveforms exhibiting small Peak Sidelobe Level (PSL). PSL shows the maximum auto-correlation sidelobe of a transmit waveform in a typical Single-Input Single-Output (SISO)/Single-Input Multiple-Output (SIMO), or phased-array radar system. If this value is not small, then either a false detection or a miss detection may happen, based on the way the Constant False Alarm

Rate (CFAR) detector is tuned [1]. In Multiple-Input Multiple-Output (MIMO) radars, PSL minimization is more complex since the cross-correlation sidelobes of transmitting set of sequences need to be also considered. Small value in cross-correlation sidelobes helps the radar receiver to separate the transmitting waveforms and form a MIMO virtual array.

Similar properties hold for Integrated Sidelobe Level (ISL) of transmitting waveforms where in case of SISO/SIMO or phased-array radars, the energy of auto-correlation sidelobes should be small to mitigate the deleterious effects of distributed clutter. In solid state-based weather radars, ISL needs to be small to enhance reflectively estimation and improve the performance of hydrometer classifier [2]. In MIMO radar systems, ISL shows the energy leakage of different waveforms in addition to the energy of non-zero auto-correlation sidelobes. Indeed, correlation sidelobes are a form of self-noise that reduce the effectiveness of transmitting waveforms in every radar system [3].

In a MIMO radar system, different multiplexing schemes are used to create zero values for cross-correlations of the transmitting waveforms, Frequency Division Multiplexing (FDM), Doppler Division Multiplexing (DDM), and Time Division Multiplexing (TDM) as some examples [4]. Currently, TDM-MIMO radars are commercialized in the automotive industry with a variety of functionalities from de-chirping and Doppler processing to angle estimation and tracking [5], [6]. However, Code Division Multiplexing (CDM)-MIMO is the next step of the industry, which can use more efficiently the available resources (time space and frequency) [7]–[9].

In this paper, we devise a method called Weighted BSUM sEquence SeT (WeBEST) to design transmitting waveforms for CDM-MIMO radars. To this end, we adopt the weighted ℓ_p-norm of auto- and cross-correlation sidelobes as the objective function and minimize it under Continuous Phase (CP) and Discrete Phase (DP) constraints. The weighting and p values in the provided formulation create a possibility for intelligent transmission based on prevailing environmental conditions, where can select appropriate p based on presence of distributed clutter or strong target [10]–[13]. For example, choosing $p \to 0$ and minimizing the ℓ_p-norm of auto- and cross-correlation sidelobes, a set of sequences with sparse sidelobes will be obtained. With $p = 2$, the resulting optimized set of sequences will have small ISL value which performs well in the presence of clutter. Further, by minimizing the ℓ_p-norm when $p \to +\infty$, the optimized set of sequence will have small PSL and are well suited for enhancing the detection of point targets.

A. Background and Related Works

Waveform design based on sidelobe reduction in SISO/SIMO or phased-array radar systems: Research into design of waveforms with small ISL and PSL values has significantly increased over the past decade for single waveform transmitting radar systems [3], [14]–[22]. In case of ISL minimization, several optimization frameworks are proposed, including power method-like iterations, Majorization-Minimization (MM), Coordinate Descent (CD), Gradient Descent (GD), Alternating Direction Method of Multipliers (ADMM), Inexact Alternating Direction Penalty Method (IADPM), Proximal Method of Multipliers (PMM) and MM-MDR to name a few [14]–[26]. In [3], an algorithm based on steepest descent is proposed for designing long binary sequences. Joint ISL and PSL minimization based on CD under DP and CP constraints is proposed in [20]. In the proposed method of this paper, ℓ_p-norm of auto-correlation sidelobes when $p \to +\infty$ is considered for the initialization. Similarly, several papers have considered ℓ_p-norm minimization to design waveform with small PSL values. In [21], a GD based approach is proposed to design sequences with small sidelobes based on ℓ_p-norm criteria for SISO radar systems. The proposed algorithm is applicable when p is an even number, i.e., $p = 2n, n \in \mathbb{Z}^+$. In [17], [18], MM based approach are proposed for ℓ_p-norm minimization when $p \geq 2$.

The results in [17], [18], [20] depict that by gradually increasing p during the minimization of the ℓ_p-norm of auto-correlation sidelobes, sequences with very small PSL values are obtained. Motivated by this observation, this paper investigates ℓ_p-norm minimization of auto- and cross-correlation functions to obtain set of sequences with very small PSL values for MIMO radars.

Waveform design based on sidelobe reduction in MIMO radar systems: In order to design set of sequences with small auto- and cross-correlation sidelobes, several approaches including Multi-Cyclic Algorithm-New (CAN)/Multi-PeCAN [27], Iterative Direct Search [28], ISLNew [29], MM-Corr [30] and CD [31]–[35], are proposed all considering the ISL as the design metric. On the other hand, few papers have focused on PSL minimization for MIMO radars [36], [37]. In [36], [38] a CD based approach is proposed to minimize PSL. In [37], [39] a MM based approach is proposed to directly minimize the PSL and design set of sequences for MIMO radar systems. The authors in [40] solve the problem based on Chebyshev distance minimization. In the current study, we design set of sequences with very small PSL values by minimizing ℓ_p-norm of auto- and cross-correlation sidelobes for a set of sequences which was not addressed previously in the literature. In contrast to the previous studies, we solve the problem for a general p value ($p > 0$)

under DP constraint, and solve it for $0 < p \leq 1 \cup p \geq 2$ under CP constraint. Interestingly, the obtained PSL values are close to the Welch lower bound and fill the gap between the best of literature and the available lower bound.

B. Contributions

The main contributions of the current article are summarized below.

- *Unified optimization framework:* We propose a unified framework based on Block Successive Upper Bound Minimization (BSUM) paradigm to solve a general ℓ_p-norm minimization problem under practical design constraints which make the problem non-convex, non-smooth and NP-hard. The proposed problem formulation includes ℓ_1/ℓ_0-norm of the auto-correlation sidelobe which relatively have lower number of local minima comparing with ℓ_2-norm. Also, the local minima of those cost function would correspond to sequences with good auto-correlation sidelobe levels. For instance, in the simulation analysis we show that any local minima of ℓ_0-norm of auto-correlation would have many zeros (sparse auto-correlation) which can enhance the detection performance in the presence of distributed clutter.
- *Entry- and vector-based solutions:* BSUM is an iterative method, that in each iteration, the variable is divided into several blocks, then the problem is optimized with respect to that block. The blocks are a portion of the variable or in the smallest case, it is one entry. In this regard, in each iteration of BSUM, we propose two approaches, i.e, entry- and vector-based solutions. In the entry-based optimization, we formulate the problem with respect to a single variable; this enables us to find the critical points and obtain the global optimum solution in each step. For vector-based optimization, we propose a solution based on GD. This approach is faster than the entry-based method. However, the entry-based method has a better performance in terms of minimizing the objective function due to obtaining the global optimum solution in each step.
- *Trade-off and flexibility:* By conducting thorough performance assessment, we propose a flexible tool to design set of sequences with different properties. We show that the ℓ_p-norm optimization framework provides the flexibly of controlling optimization objective by choosing p, where $p \to \infty$ leads to design set of waveforms with good PSL property. Choosing $p \to 0$ leads to sparse auto- and cross-correlation and choosing $p = 2$ leads to design set of waveforms with good ISL property.

While BSUM offers a generic framework, the contribution of the paper lies in devising different solutions based on simplifying the complexity and obtain a good performance. We finally propose a direct solution for the discrete phase constraint using Fast Fourier Transform (FFT) technique.

C. Organization and Notations

The rest of this paper is organized as follows. In Section II, we formulate the ℓ_p-norm minimization for MIMO radar systems, then we introduce the BSUM method as the Optimization framework and finally we define the local approximation functions suitable for ℓ_p-norm problem. We develop the BSUM framework to solve the problem in Section III and provide numerical experiments to verify the effectiveness of proposed algorithm in Section IV.

Notations: This paper uses lower-case and upper-case boldface for vectors ($\mathbf{a}$) and matrices ($\mathbf{A}$) respectively. The set of complex, positive integer numbers, transpose, conjugate transpose, sequence reversal, Frobenius norm, ℓ_p norm, absolute value, round operator, real part, imaginary part, Hadamard product and cross-correlation operator are denoted by $\mathbb{C}$, $\mathbb{Z}^+$, $(.)^T$, $(.)^H$, $(.)^r$, $\|.\|_F$, $\|.\|_p$, $|.|$, $\lfloor . \rceil$, $\Re(a)$, $\Im(a)$, $\odot$ and $\circledast$ symbols respectively. The letter j represents the imaginary unit (i.e., $j = \sqrt{-1}$), while the letter (i) is used as step of a procedure.

II. Problem Formulation

We consider a narrow-band MIMO radar system with M transmitters and each transmitting a sequence of length N in the fast-time domain. Let the matrix $\boldsymbol{X} \in \mathbb{C}^{M\times N}$ denote the set of transmitted sequences in baseband, whose the m^{th} row indicates the N samples of m^{th} transmitter while the n^{th} column indicates the n^{th} time-sample across the M transmitters. Let $\mathbf{x}_m \triangleq [x_{m,1}, x_{m,2}, \ldots, x_{m,N}]^T \in \mathbb{C}^N$ be the transmitted signal from m^{th} transmitter. The aperiodic cross-correlation of $\mathbf{x}_m$ and $\mathbf{x}_l$ is defined as,

$$r_{m,l}(k) \triangleq (\mathbf{x}_m \circledast \mathbf{x}_l)_k = \sum_{n=1}^{N-k} x_{m,n} x_{l,n+k}^*, \tag{1}$$

where $m, l \in \{1, \ldots, M_t\}$ are the transmit antennas indices and $k \in \{-N+1, \ldots, N-1\}$ is the lag of cross-correlation. If $m = l$, (1) represents the aperiodic auto-correlation of signal $\mathbf{x}_m$. The zero lag of auto-correlation ($r_{m,m}(0)$) represent the peak of the m^{th} matched filter output. Also $|r_{m,m}(0)|$ contains the energy of sequence which for constant modulus sequences is equal to N. The other lags ($k \neq 0$) are referred to the sidelobes. The weighted ℓ_p-norm of auto- and cross correlation in MIMO radar is written as,

$$\left(\sum_{m=1}^{M} \sum_{l=1}^{M} \sum_{k=-N+1}^{N-1} |w_k r_{m,l}(k)|^p - M(w_0 N)^p \right)^{\frac{1}{p}}, \tag{2}$$

where

$$w_k = \begin{cases} 1, & k \in \mathcal{V} \\ 0, & k \in \mathcal{U} \end{cases}$$

with $\mathcal{V}$ and $\mathcal{U}$ are the desired and undesired correlation lags, respectively, that satisfy $\mathcal{V} \cup \mathcal{U} = \{-N+1, \ldots, N-1\}$ and $\mathcal{V} \cap \mathcal{U} = \emptyset$ [1]. The $M(w_0 N)^p$ term in (2) is the weighted ℓ_p-norm of the mainlobes, where $\sum_{m=1}^{M} |w_0 r_{m,m}(0)|^p = M(w_0 N)^p$. Since the term $M(w_0 N)^p$ in (2) is constant, the weighted ℓ_p-norm minimization is equivalently written as,

$$\begin{cases} \min\limits_{\mathbf{X}} & f(\mathbf{X}) \triangleq \sum_{m=1}^{M} \sum_{l=1}^{M} \sum_{k=-N+1}^{N-1} |w_k r_{m,l}(k)|^p \\ s.t. & x_{m,n} \in \mathcal{X}_\infty \quad \text{or} \quad \mathcal{X}_L, \end{cases} \tag{3}$$

where, $\mathcal{X}_\infty$ and $\mathcal{X}_L$ indicating the unimodular and discrete phase with L alphabet size sequences. More precisely, we consider $\mathcal{X}_\infty = \{e^{j\phi} | \phi \in \Omega_\infty\}$ and $\mathcal{X}_L = \{e^{j\phi} | \phi \in \Omega_L\}$, where $\Omega_\infty \triangleq (-\pi, \pi]$ and $\Omega_L \triangleq \{0, \frac{2\pi}{L} \ldots, \frac{2\pi(L-1)}{L}\}$. The unimodular and discrete phase are equality constraint and they are not an affine set. Therefore the optimization problem is non-convex, multi-variable and NP-hard in general. Note that, due to the existence of the parameter p in $f(\mathbf{X})$, direct solution of (3) is complicated.

III. Proposed Method

In this paper, we propose a method based on BSUM framework to tackle the non-convex problem (3). The BSUM framework provides a connection between Block Coordinate Descent (BCD) and MM, by successively optimizing a certain upper bound of the original objective in a coordinate wise manner [2]. In this context, BSUM requires to find an approximation function for the objective function in (3), and then the approximation function should be written in a simplified form with respect to one variable block while other blocks are held fixed. In this regard, term $|w_k r_{m,l}(k)|^p$ in (3) is majorized by the following local approximation functions (see Appendix A for more details),

$$u(w_k r_{m,l}(k)) = \eta_{mlk} |w_k r_{m,l}(k)|^2 + \psi_{mlk} |w_k r_{m,l}(k)| + \nu_{mlk} \tag{4}$$

where[3],

[1] Mathematically, one can select $w_k \geq 0$ and still use the method described here to solve the problem.

[2] Details of BSUM and different ways of choosing approximation functions of this paper can be found in Appendix A.

[3] We do not report the value of ν_{mlk} because it is a constant term that has no effect on the optimization procedure.

$$\eta_{mlk} \triangleq \begin{cases} \dfrac{\tau^p + (p-1)|w_k r_{m,l}^{(i)}(k)|^p - p\tau|w_k r_{m,l}^{(i)}(k)|^{p-1}}{(\tau - |w_k r_{m,l}^{(i)}(k)|)^2} & p \geq 2 \\ \begin{cases} \dfrac{p\epsilon^{(p-2)}}{2} & |w_k r_{m,l}(k)| \leqslant \epsilon \\ \dfrac{p|w_k r_{m,l}(k)|^{(p-2)}}{2} & |w_k r_{m,l}(k)| > \epsilon \end{cases} & 0 < p \leq 1, \end{cases}, \quad \tau \triangleq \left(\sum_{-N-1}^{N-1} |w_k r_{m,l}^{(i)}(k)|^p \right)^{\frac{1}{p}} \tag{5}$$

and

$$\psi_{mlk} \triangleq \begin{cases} p|w_k r_{m,l}^{(i)}(k)|^{p-1} - 2\eta_{mlk}|w_k r_{m,l}^{(i)}(k)| & p \geq 2 \\ 0 & 0 < p \leq 1. \end{cases} \tag{6}$$

In (5), ϵ is a positive and small value ($\epsilon > 0$ and $\epsilon \to 0$) incorporated in the objective function to avoid the singularity problem for $0 < p \leq 1$.

Consequently, (3) is equivalently replaced with,

$$\mathcal{P} \begin{cases} \min\limits_{\mathbf{X}} & u(\mathbf{X}) \triangleq \sum_{m=1}^{M} \sum_{l=1}^{M} \sum_{k=-N+1}^{N-1} u(w_k r_{m,l}(k)) \\ s.t. & x_{m,n} \in \mathcal{X}_\infty \quad \text{or} \quad \mathcal{X}_L, \end{cases} \tag{7}$$

Let $\mathbf{x}_t$ ($t \in \{1, \ldots, M\}$) be the only variable block, while other blocks are held fixed and stored in the matrix $\mathbf{X}_{-t} \triangleq [\mathbf{x}_1^T; \ldots; \mathbf{x}_{t-1}^T; \mathbf{x}_{t+1}^T; \ldots; \mathbf{x}_M^T] \in \mathbb{C}^{(M-1)\times N}$. In this case, the approximation function $u(\mathbf{X})$ is decomposed to a term independent of the optimization variable $\mathbf{x}_t$, and two other terms, one indicating the auto-correlation of $\mathbf{x}_t$, and the other is its cross-correlation with the other sequences of the set $\mathbf{X}_{-t}$. Precisely,

$$u(\mathbf{X}) = u_m(\mathbf{X}_{-t}) + u_{au}(\mathbf{x}_t) + u_{cr}(\mathbf{x}_t, \mathbf{X}_{-t}), \tag{8}$$

where

$$\begin{aligned} &u_m(\mathbf{X}_{-t}) = \sum_{\substack{m,l=1 \\ m,l\neq t}}^{M} \sum_{k=-N+1}^{N-1} u(w_k r_{m,l}(k)), \quad u_{au}(\mathbf{x}_t) = \sum_{k=-N+1}^{N-1} u(w_k r_{t,t}(k)), \\ &u_{cr}(\mathbf{x}_t, \mathbf{X}_{-t}) = 2 \sum_{\substack{l=1 \\ l\neq t}}^{M} \sum_{k=-N+1}^{N-1} u(w_k r_{t,l}(k)). \end{aligned} \tag{9}$$

In the sequel, we provide different approaches for minimizing $u(\mathbf{X})$ under the aforementioned constraints.

A. Code entry optimization

To design the code vector $\mathbf{x}_t$, one possible solution is to optimize its code entry sequentially. Let $x_{t,d}$ ($t \in \{1, \ldots, M\}$ and $d \in \{1, \ldots, N\}$) be the only entry variable of vector $\mathbf{x}_t$ while other entries are held fixed and stored in vector $\mathbf{x}_{t,-d} \triangleq [x_{t,1}, \ldots, x_{t,d-1}, 0, x_{t,d+1}, \ldots, x_{t,N}]^T \in \mathbb{C}^N$.

In this regard, the auto- and cross-correlation of t^{th} transmitter is written as d^{th} entry as follows, [20], [31], [36],

$$r_{t,t}(k) \triangleq \bar{c}_{ttdk} + \bar{a}_{ttdk} x_{t,d} + \bar{b}_{ttdk} x_{t,d}^*, \quad r_{t,l}(k) \triangleq \bar{c}_{tldk} + \bar{a}_{tldk} x_{t,d}, \tag{10}$$

where,

$$\begin{aligned} &\bar{c}_{tldk} \triangleq \sum_{\substack{n=1 \\ n\neq d}}^{N-k} x_{t,n} x_{l,n+k}^*, \bar{a}_{tldk} \triangleq x_{l,d+k}^* I_A(d+k), \quad \bar{c}_{ttdk} \triangleq \sum_{\substack{n=1 \\ n\neq d, n\neq d-k}}^{N-k} x_{t,n} x_{t,n+k}^*, \\ &\bar{a}_{ttdk} \triangleq x_{t,d+k}^* I_A(d+k), \bar{b}_{ttdk} \triangleq x_{t,d-k} I_A(d-k), \end{aligned} \tag{11}$$

where, $I_A(p)$ is the indicator function of set $A = \{1, \ldots, N\}$, i.e, $I_A(p) \triangleq \begin{cases} 1, & p \in A \\ 0, & p \notin A \end{cases}$. Please note that the coefficients $\bar{c}_{tldk}$ and $\bar{c}_{ttdk}$ depend on $\mathbf{x}_{t,-d}$ while $\bar{a}_{tldk}$, $\bar{a}_{ttdk}$ and $\bar{b}_{ttdk}$ depend on $x_{t,d}$. Therefore the weighted auto- and cross-correlation of t^{th} transmitter becomes,

$$w_k r_{t,t}(k) = c_{ttdk} + a_{ttdk} x_{t,d} + b_{ttdk} x_{t,d}^* \quad w_k r_{t,l}(k) = c_{tldk} + a_{tldk} x_{t,d}, \tag{12}$$

where

$$a_{ttdk} \triangleq w_k \bar{a}_{ttdk}, \; b_{ttdk} \triangleq w_k \bar{b}_{ttdk}, \; c_{ttdk} \triangleq w_k \bar{c}_{ttdk}, \; a_{tldk} \triangleq w_k \bar{a}_{tldk}, \; c_{tldk} \triangleq w_k \bar{c}_{tldk}. \tag{13}$$

Further, to consider the unimodularity constraint, we substitute $x_{t,d}$ with $e^{j\phi}$. In this case, it is shown that,

$$w_k r_{t,t}(k,\phi) = c_{ttdk} + a_{ttdk} e^{j\phi} + b_{ttdk} e^{-j\phi}, \quad w_k r_{t,l}(k,\phi) = c_{tldk} + a_{tldk} e^{j\phi}. \tag{14}$$

Observe that the term $u_m(\mathbf{X}_{-t})$ in (8) is independent to the optimization variable $x_{t,d}$. Thus, the optimization problem (7) with respect to $x_{t,d}$ becomes,

$$\begin{cases} \min\limits_{\phi} & \sum_{k=-N+1}^{N-1} u(w_k r_{t,t}(k,\phi)) + 2 \sum_{\substack{l=1 \\ l\neq t}}^{M} \sum_{k=-N+1}^{N-1} u(w_k r_{t,l}(k,\phi)) \\ s.t. & \phi \in \Omega_\infty, \end{cases} \tag{15}$$

In this case, by some mathematics manipulation, the objective function in (15) is explicitly written based on ϕ as (see Appendix B),

$$\mathcal{P}_e \begin{cases} \min\limits_{\phi} & u(\phi) \triangleq \Re\left\{ \sum_{n=-2}^{2} v_n e^{jn\phi} \right\} \\ s.t. & \phi \in \Omega_\infty, \end{cases} \tag{16}$$

where the coefficients v_n are defined in Appendix B.

The solution to $\mathcal{P}_e$ is calculated by finding the critical points of the problem and selecting the solution that minimizes the objective. In this regard, we find the real roots of the first-order derivative of the objective function and evaluate the objective function in these points and the boundaries and select the solution that minimizes the objective. In this regard, the derivative of $u(\phi)$ is obtained by,

$$u'(\phi) = \Re\left\{ j \sum_{n=-2}^{2} n v_n e^{jn\phi} \right\}, \tag{17}$$

Then, considering trigonometric equations of $\cos(\phi) = (1-\tan^2(\frac{\phi}{2}))/(1+\tan^2(\frac{\phi}{2}))$, $\sin(\phi) = 2\tan(\frac{\phi}{2})/(1+\tan^2(\frac{\phi}{2}))$ and performing the change of variable $z \triangleq \tan(\frac{\phi}{2})$ in (17), it is shown that finding the roots of $\frac{du(\phi)}{d\phi} = 0$ is equivalent to finding the roots of the following 4 degree real polynomials (see Appendix C for details),

$$\sum_{k=0}^{4} s_k z^k = 0, \tag{18}$$

where the coefficients are given in Appendix C.

We only admit the real roots for (18). Let us assume that z_k ($k = \{1, \ldots, 4\}$) be the roots of $\sum_{k=0}^{4} s_k z^k = 0$. Hence, the critical points of $u(\phi)$ are expressed as,

$$\Omega_u = \left\{ 2\arctan(z_k) | \Im(z_k) = 0 \right\} \tag{19}$$

Therefore, the optimum phase would be,

$$\phi^\star = \arg\min_{\phi} \left\{ u(\phi) | \phi \in \Omega_u \right\}. \tag{20}$$

Subsequently the optimum solution for $x_{t,d}$ at i^{th} iteration is, $x_{t,d}^{(i+1)} = e^{j\phi^\star}$.

Remark 1: Since, $u(\phi)$ is functions of $\cos\phi$ and $\sin\phi$, it is periodic, real and differentiable. Therefore, it has at least two extrema and hence its derivative has at least two real roots; thus Ω_u never becomes a null set. As a result in each iteration, the problem has a solution and never becomes infeasible.

Remark 2: To design a sequence with discrete phase constraint, an elegant solution is obtained for $0 < p < \infty$ by using FFT as detailed below. In this case, the optimization problem with respect to the phase variable ϕ by removing the constant terms is written as,

$$\mathcal{P}_d \begin{cases} \min\limits_{\phi} & 2\sum\limits_{\substack{l=1 \\ l\neq t}}^{M} \sum\limits_{k=-N+1}^{N-1} |c_{tldk} + a_{tldk} e^{j\phi}|^p + \sum\limits_{k=-N+1}^{N-1} |c_{ttdk} + a_{ttdk} e^{j\phi} + b_{ttdk} e^{-j\phi}|^p \\ s.t. & \phi \in \Omega_L, \end{cases} \tag{21}$$

Note that in the optimization problem (21), all the discrete points lie on the boundary of the optimization problem; hence, all of them are critical points for the problem. Interestingly, the

solution to (21) is obtained efficiently using an FFT operation due to the fact that the objective function represents the modulus of the L-point Discrete Fourier Transform (DFT) of a sequence associated with coefficients c_{ttdk}, a_{ttdk}, b_{ttdk}, c_{tldk}, and a_{tldk}. Precisely, we find the index $l'^{\star}$ by (see Appendix D),

$$l'^{\star} = \arg \min_{l=1,\dots,L} 2\sum_{\substack{l=1 \\ l\neq t}}^{M} \sum_{k=-N+1}^{N-1} |\mathcal{F}_L\{a_{tldk}, c_{tldk}\}|^p + \sum_{k=-N+1}^{N-1} |\mathcal{F}_L\{a_{ttdk}, c_{ttdk}, b_{ttdk}\}|^p, \quad (22)$$

where, F_L is L-point DFT operator. Hence, the optimum phase is

$$\phi^{\star} = \frac{2\pi(l'^{\star} - 1)}{L}. \quad (23)$$

Subsequently, the optimum entry is $x_{t,d}^{(i+1)} = e^{j\phi^{\star}}$.

The summary of the proposed method, called WeBEST-entry based design optimization framework is given by **Algorithm 1**, where, $x_{t,d}^{(i+1)} = e^{j\phi^{\star}}$ is the optimized solution. To obtain this solution, WeBEST-e (entry optimization) considers a feasible set of sequences as the initial waveforms. Then, at each iteration, it selects $x_{t,d}$ as the variable and updates that with optimized $x_{t,d}^{\star}$, denoted by $x_{t,d}^{(i+1)}$. This procedure is repeated for other entries and is undertaken until all the entries are optimized at least once. After optimizing the MN^{th} entry, the algorithm examines the convergence metric for the objective function. If the stopping criterion is not met the algorithm repeats the aforementioned steps.

B. Code vector optimization

One alternative approach to solve (7) and minimize $u(\mathbf{X})$ is to consider the entire code vector $\mathbf{x}_t$ as the optimization variable. Let $\mathbf{\Phi} \triangleq \angle\mathbf{X} \in \mathbb{R}^{M\times N}$, $\mathbf{\Phi}_{-t} \triangleq \angle\mathbf{X}_{-t} \in \mathbb{R}^{(M-1)\times N}$ and $\boldsymbol{\varphi}_t \triangleq \angle\mathbf{x}_t \in \mathbb{R}^N$ be the phases corresponding to the matrices $\mathbf{X}$, $\mathbf{X}_{-t}$ and the vector variable $\mathbf{x}_t$ respectively. Hence, with respect to $\boldsymbol{\varphi}_t$, the optimization problem is

$$\begin{cases} \min\limits_{\boldsymbol{\varphi}_t} & u_m(\mathbf{\Phi}_{-t}) + u_{au}(\boldsymbol{\varphi}_t) + u_{cr}(\boldsymbol{\varphi}_t, \mathbf{\Phi}_{-t}) \\ s.t. & \phi_{t,n} \in \Omega_{\infty}. \end{cases} \quad (24)$$

To solve (24), one possible solution is to use GD framework, which is a first-order iterative optimization algorithm for finding a local minimum of a differentiable function. In general, the GD procedure starts with an initial solution ($\mathbf{\Phi}^{(0)}$), then at i^{th} iteration, each block ($\boldsymbol{\varphi}_t$) is updated by the following equation [41],

$$\boldsymbol{\varphi}_t^{(i+1)} = \boldsymbol{\varphi}_t^{(i)} + \delta^{(i)}\Delta\boldsymbol{\varphi}_t^{(i)} \quad (25)$$

Input: Initial set of feasible sequences, $\mathbf{X}^{(0)}$.
Initialization: $i := 0$.
Optimization:
1) **while**, $\Delta\mathbf{X}^{(i+1)} \triangleq \left\|\mathbf{X}^{(i+1)} - \mathbf{X}^{(i)}\right\|_F \leq \zeta$ **do**
2) $\mathbf{X}^{(i+1)} = \mathbf{X}^{(i)}$;
3) **for** $t = 1, \ldots, M$ **do**
4) **for** $d = 1, \ldots, N$ **do**
5) Optimize $x_{t,d}$:
a) with CP:
i) From Appendix C calculate the coefficients s_k in (18);
ii) Find the roots of (18), $\sum_{k=0}^{4} s_k z^k = 0$ and save it as z_k;
iii) Find the real critical points using (19), $\Omega_u = \left\{2\arctan(z_k) | \Im(z_k) = 0\right\}$;
iv) Derive the optimum phase using (20), $\phi^\star = \arg\min_\phi \left\{u(\phi) | \phi \in \Omega_u\right\}$;
b) with DP:
i) Derive the optimum index of M-ary Phase Shift Keying (MPSK) alphabet using (22),
$l'^\star = \arg\min_{l=1,\ldots,L} 2\sum_{\substack{l=1 \\ l\neq t}}^{M}\sum_{k=-N+1}^{N-1} |\mathcal{F}_L\{a_{tldk}, c_{tldk}\}|^p + \sum_{k=-N+1}^{N-1} |\mathcal{F}_L\{a_{ttdk}, c_{ttdk}, b_{ttdk}\}|^p$;
ii) Derive the optimum phase using $\phi^\star = \frac{2\pi(l'^\star - 1)}{L}$;
6) Update $x_{t,d}^{(i+1)} = e^{j\phi^\star}$;
7) $\mathbf{X}^{(i+1)} = \mathbf{X}^{(i+1)}|_{x_{t,d}=x_{t,d}^{(i+1)}}$;
8) **end for**
9) **end for**
10) $i := i + 1$;
11) **end while**
Output: $\mathbf{X}^\star = \mathbf{X}^{(i+1)}$.

Algorithm 1: :WeBEST-entry optimization framework

where, $\delta^{(i)}$ and $\Delta\boldsymbol{\varphi}_t^{(i)}$ are the *step size* (*step length*) and the *search direction* at i^{th} iteration, respectively. After updating all of the blocks, the phase matrix is updated by $\boldsymbol{\Phi}^{(i+1)} \triangleq [\boldsymbol{\varphi}_1^{(i+1)}, \ldots, \boldsymbol{\varphi}_M^{(i+1)}]^T$. In gradient descent method, the search direction is equal to the opposite direction of the gradient i.e. $\Delta\boldsymbol{\varphi}_t^{(i)} = -\nabla u(\boldsymbol{\varphi}_t^{(i)})$. Note that, the convergence behavior of GD methods is highly dependent on choosing the step size and the step direction. In order to achieve the monotonic descent behavior in each step ($u(\boldsymbol{\varphi}_t^{(i+1)}) \leq u(\boldsymbol{\varphi}_t^{(i)})$), *backtracking line search* is used for choosing the step size, where it depends on two constants α and β with $0 < \alpha < 0.5$ and $0 < \beta < 1$, indicated in **Algorithm 2** [41].

Algorithm 3, called WeBEST-v shows the procedure of vector optimization of ℓ_p-norm minimization. In this algorithm, matrix $\nabla\boldsymbol{\Phi}^{(i)} \in \mathbb{R}^{M\times N}$ contains the gradient of objective function

Input: $\Delta\boldsymbol{\varphi}_t^{(i)}$, α $(0<\alpha<0.5)$ and β $(0<\beta<1)$.
Initialization: $\delta^{(i)}:=1$
1) **while** $f(\boldsymbol{\varphi}_t^{(i)}+\delta^{(i)}\Delta\boldsymbol{\varphi}_t^{(i)})>f(\boldsymbol{\varphi}_t^{(i)})+\alpha s\nabla f(\boldsymbol{\varphi}_t^{(i)})\Delta\boldsymbol{\varphi}_t^{(i)}$
2) $\quad\delta^{(i)}:=\delta^{(i)}\beta$;
3) **end while**

Algorithm 2: : Backtracking line search

Input: $\mathbf{X}^{(0)}$
Initialization: $i:=0$, $\boldsymbol{\Phi}^{(i)}=\angle\mathbf{X}^{(0)}$.
1) **while**, $\Delta\mathbf{X}^{(i+1)}\triangleq\left\|\mathbf{X}^{(i+1)}-\mathbf{X}^{(i)}\right\|_F\leq\zeta$ **do**
2) $\quad$**for** $t:=1:M$
3) $\quad\quad\Delta\boldsymbol{\varphi}_t^{(i)}:=-\nabla_{\boldsymbol{\varphi}_t}u(\boldsymbol{\varphi}_t^{(i)})$;
4) $\quad\quad$obtain $\delta^{(i)}$ using backtracking line search;
5) $\quad\quad\boldsymbol{\varphi}_t^{(i+1)}:=\boldsymbol{\varphi}_t^{(i)}+\delta^{(i)}\Delta\boldsymbol{\varphi}_t^{(i)}$;
6) $\quad$**end for**
7) $\quad\quad i:=i+1$;
8) **end while**

Algorithm 3: : WeBEST-vector optimization framework

with respect to sequence phases at i^{th} iteration, i.e., $\nabla\boldsymbol{\Phi}^{(i)}\triangleq[\nabla_{\boldsymbol{\varphi}_1}u(\boldsymbol{\varphi}_1^{(i)}),\ldots,\nabla_{\boldsymbol{\varphi}_M}u(\boldsymbol{\varphi}_M^{(i)})]^T$. This procedure will be continued until the algorithm meet the stopping criteria .

Algorithm 3 requires calculation of the gradients of $\nabla_{\boldsymbol{\varphi}_t}u(\boldsymbol{\varphi}_t^{(i)})$, which is obtained using the following lemma.

Lemma 3.1: The gradient of $\nabla_{\boldsymbol{\varphi}_t}u(\boldsymbol{\varphi}_t^{(i)})$ is equal to,

$$\begin{aligned}\nabla_{\boldsymbol{\varphi}_t}u(\boldsymbol{\varphi}_t^{(i)})=4\Im\{\mathbf{x}_t^*\odot((\boldsymbol{\vartheta}_{tt}^2\odot(\mathbf{x}_t\circledast\mathbf{x}_t))\circledast\mathbf{x}_t)_{k+N-1}\}\\+4\textstyle\sum_{\substack{l=1\\l\neq t}}^{M}\Im\{\mathbf{x}_t^*\odot((\boldsymbol{\vartheta}_{tl}^2\odot(\mathbf{x}_l\circledast\mathbf{x}_t)^r)\circledast\mathbf{x}_l^*)_{k+N-1}\},\end{aligned}\tag{26}$$

where, $\boldsymbol{\vartheta}_{tt}\triangleq[\vartheta_{tt}(-N+1),\ldots,\vartheta_{tt}(N-1)]^T|\vartheta_{tt}(k)\triangleq w_k\sqrt{\mu_{ttk}}$, $\mu_{ttk}\triangleq\frac{p}{2}|w_kr_{t,t}^{(i)}(k)|^{p-2}$ and $\boldsymbol{\vartheta}_{tl}\triangleq[\vartheta_{tl}(-N+1),\ldots,\vartheta_{tl}(N-1)]^T|\vartheta_{tl}(k)\triangleq w_k\sqrt{\mu_{tlk}}$, $\mu_{tlk}\triangleq\frac{p}{2}|w_kr_{t,l}^{(i)}(k)|^{p-2}$.

proof: Since the third term in (4) is a constant, it does not affect the gradient calculation and it can be removed. Beside, according to lemma A.3, the ℓ_1-norm in the second term ($|w_kr_{m,l}(k)|$) is majorized by the following equation [42],

$$\frac{1}{2}|w_kr_{m,l}^{(i)}(k)|^{-1}|w_kr_{m,l}(k)|^2-\frac{1}{2}|w_kr_{m,l}^{(i)}(k)|.\tag{27}$$

Substituting (27) with the $|w_kr_{m,l}(k)|$ term in (4), becomes,

$$\bar{u}(w_kr_{m,l}(k))\triangleq\mu_{mlk}|w_kr_{m,l}(k)|^2+\varsigma_{mlk},\tag{28}$$

where,

$$\begin{aligned}\mu_{mlk} &\triangleq \frac{p}{2}|w_k r_{m,l}^{(i)}(k)|^{p-2} \\ \varsigma_{mlk} &\triangleq \eta_{mlk}|w_k r_{m,l}^{(i)}(k)|^2 - \frac{1}{2}\psi_{mlk}|w_k r_{m,l}^{(i)}(k)| - (p-1)|w_k r_{m,l}^{(i)}(k)|^p,\end{aligned} \tag{29}$$

Now we define $\bar{u}(\mathbf{\Phi}) \triangleq u_m(\mathbf{\Phi}_{-t}) + \bar{u}_{au}(\boldsymbol{\varphi}_t) + \bar{u}_{cr}(\boldsymbol{\varphi}_t, \mathbf{\Phi}_{-t})$, where,

$$\bar{u}_{au}(\boldsymbol{\varphi}_t) = \sum_{k=-N+1}^{N-1}\left(\mu_{ttk}|w_k r_{t,t}(k)|^2 + \varsigma_{ttk}\right) = \left\|\boldsymbol{\varrho}_{tt} \odot (\mathbf{x}_t \circledast \mathbf{x}_t)_k\right\|_2^2 + \sum_{k=-N+1}^{N-1}\varsigma_{ttk}, \tag{30}$$

and,

$$\begin{aligned}\bar{u}_{cr}(\boldsymbol{\varphi}_t, \mathbf{\Phi}_{t-1}) &= 2\sum_{\substack{l=1\\l\neq t}}^{M}\sum_{k=-N+1}^{N-1}\left(\mu_{tlk}|w_k r_{t,l}(k)|^2 + \varsigma_{tlk}\right) \\ &= 2\sum_{\substack{l=1\\l\neq t}}^{M}\left\|\boldsymbol{\varrho}_{tl} \odot (\mathbf{x}_l \circledast \mathbf{x}_t)_k\right\|_2^2 + 2\sum_{\substack{l=1\\l\neq t}}^{M}\sum_{k=-N+1}^{N-1}\varsigma_{tlk}.\end{aligned} \tag{31}$$

The second terms in (30) and (31) are constant and can be ignored. In this regard, it is shown that [21],

$$\nabla_{\boldsymbol{\varphi}_t}\left\|\boldsymbol{\varrho}_{tt} \odot (\mathbf{x}_t \circledast \mathbf{x}_t)_k\right\|_2^2 = 4\Im\{\mathbf{x}_t^* \odot ((\boldsymbol{\varrho}_{tt}^2 \odot (\mathbf{x}_t \circledast \mathbf{x}_t)) \circledast \mathbf{x}_t)_{k+N-1}\} \tag{32}$$

$$\nabla_{\boldsymbol{\varphi}_t}\left\|\boldsymbol{\varrho}_{tl} \odot (\mathbf{x}_l \circledast \mathbf{x}_t)_k\right\|_2^2 = 2\Im\{\mathbf{x}_t^* \odot ((\boldsymbol{\varrho}_{tl}^2 \odot (\mathbf{x}_l \circledast \mathbf{x}_t)^r) \circledast \mathbf{x}_l^*)_{k+N-1}\} \tag{33}$$

Please note that, since $\bar{u}(\mathbf{\Phi})$ majorizes the $|w_k r_{m,l}(k)|$ term of $u(\mathbf{\Phi})$, therefore according to the MM properties the gradient of $\bar{u}(\mathbf{\Phi})$ is equal to $u(\mathbf{\Phi})$ at $\boldsymbol{\varphi}_t$ i.e. $\nabla_{\boldsymbol{\varphi}_t}\bar{u}(\mathbf{\Phi}) = \nabla_{\boldsymbol{\varphi}_t}u(\mathbf{\Phi})$. Likewise, $\bar{u}(\mathbf{\Phi})$ is a majorizer function for $f(\mathbf{\Phi})$, thus, $\nabla_{\boldsymbol{\varphi}_t}\bar{u}(\mathbf{\Phi}) = \nabla_{\boldsymbol{\varphi}_t}u(\mathbf{\Phi}) = \nabla_{\boldsymbol{\varphi}_t}f(\mathbf{\Phi})$.

Therefore, considering the equations (32), (33), (30) and (31) readily the gradient in (26) is obtained which completes the proof.

C. Convergence

The convergence of the proposed method can be discussed in two aspects, the convergence of objective function and the convergence of the waveform set $\mathbf{X}$. With regard to the objective function, as $u(\mathbf{X}) > 0$, therefore, this expression is also valid for the optimum solution of WeBEST-e and WeBEST-v ($u(\mathbf{X}^\star) > 0$). On the other hand, both WeBEST-e and WeBEST-v minimize the objective function in each step leading to a monotonic decrease of the function value. Since the function value is lower bounded, it can be argued that the algorithm converges to a specific value. Particularly, if the algorithm starts with feasible $\mathbf{X}^{(0)}$ we have,

$$u(\mathbf{X}^{(0)}) \geqslant \cdots \geqslant u(\mathbf{X}^{(i)}) \geqslant \cdots \geqslant u(\mathbf{X}^\star) > 0,$$

The convergence of the argument requires additional conditions and its investigation is beyond the scope of this paper. However, for the optimization problem considered in this paper, we numerically observed that the argument converges as well as objective function.

D. Computational Complexity

In this subsection we evaluate the computational complexity of WeBEST-e and WeBEST-v

Complexity of WeBEST-e: This algorithm needs to perform the following steps in each iteration:

- *Calculate the coefficient* v_n *in* (16): The maximum complexity of the coefficients are belong to v_{-1}, v_0 and v_1 (see Appendix B for details). Without loss of generality, we consider $\tilde{v}_{-1} \triangleq 2\sum_{\substack{l=1\\l\neq t}}^{M}\sum_{k=-N+1}^{N-1}\eta_{tlk}a^{*}_{tldk}c_{tldk}$ to obtain the computational complexity. As can be seen, $\tilde{v}_{-1}$ needs to calculate the terms η_{tlk}, a_{tldk} and c_{tldk}. Through these three terms, c_{tldk} is the most complex term (see (11) and (13) for details), which substantially is the cross-correlation of t^{th} and l^{th} transmitters. Thus, calculating c_{tldk} requires $N\log_2(N)$ operations due to using fast convolution [43]. In addition, calculating $\tilde{v}_{-1}$ needs MN summation. Therefore $\tilde{v}_{-1}$ needs $MN^2\log_2(N)$ operation in overall. Using a recursive equation, the computational complexity can be reduced more.
- *Solving the optimization problem* (16): WeBEST-e needs finding the roots of 4 degree polynomials[4] in (18), which take 4^3 operations. In case of discrete phase constraint we obtain (22) using two L-points FFT which each has $L\log_2(L)$ operations.
- *Optimizing all the entries of matrix* $\mathbf{X}$: To this end we need to repeat the two aforementioned steps MN times.

Let us assume that $\mathcal{K}$ iterations are required for convergence of the algorithm. Therefore, the overall computational complexity of WeBEST-e is $\mathcal{O}(\mathcal{K}MN(4^3+MN^2\log_2(N)))$, for continuous phase constraint, while under discrete phase constraint is $\mathcal{O}(\mathcal{K}MN(L\log_2(L)+MN^2\log_2(N)))$.

Complexity of WeBEST-v: This algorithm needs to perform the following steps in each iteration:

- *Calculate the gradient of auto- and cross-correlation*: The gradient in (26) is expressed in terms of correlations; therefore the gradient needs $N\log_2(N)$ operation due to using fast convolution [21]. Since we need to calculate the gradient of auto-correlation for one time and cross-correlation for $M-1$ times, therefore the overall computational complexity would be $MN\log_2(N)$.

[4]For finding the roots of polynomial we use "roots" function in MATLAB. This function is based on computing the eigenvalues of the companion matrix. Thus the computational complexity of this method is $\mathcal{O}(k^3)$, where k is the degree of the polynomial [44], [45]

- *Obtain the step size*: This step contains calculating the auto- and cross-correlation part of objective functions i.e. $f_{au}(\mathbf{X})$ and $f_{cr}(\mathbf{X})$, which needs $MN\log_2(N)$ operations. Lets assume that this step needs $\mathcal{S}$ iteration to find the step size, therefore the complexity of this step would be $\mathcal{S}MN\log_2(N)$.
- *Optimizing all the entries of matrix* $\mathbf{X}$: To this end we need to repeat the two aforementioned steps M times.

Let us assume that $\mathcal{K}$ iterations are required for convergence of the WeBEST-v. Therefore, the overall computational complexity of WeBEST-v is $\mathcal{O}(\mathcal{K}\mathcal{S}M^2N\log_2(N))$.

IV. Numerical Results

In this section, we provide representative numerical examples to illustrate the effectiveness of the proposed algorithmic framework. We consider $\Delta\mathbf{X}^{(i+1)} \triangleq \left\|\mathbf{X}^{(i+1)}-\mathbf{X}^{(i)}\right\|_F \leq \zeta$ as the stopping criterion of WeBEST-e and WeBEST-v, where ζ is the stopping threshold ($\zeta > 0$). We set $\zeta = 10^{-9}$ for all the following numerical examples. We further stop the algorithm if number of iterations exceed 10^5. Also, we consider $\epsilon = 0.05$ in (5). In this section, by $L \to \infty$ we denote a set of continuous phase sequences or a set of sequences with infinity alphabet sizes. Besides, we use $10\log(.)$ to report the results based on decibel scale.

A. Convergence

Fig. 1 depicts the convergence time (behavior) of the proposed method. We consider a set of random MPSK sequences ($\mathbf{X}_0 \in \mathbb{C}^{M\times N}$) with $M = 4$ transmitters, $N = 64$ code-length, and $L = 8$ alphabet size, as the initial waveform set. For the initialization sequences, every code entry is given by,

$$x_{m,n}^{(0)} = e^{j\frac{2\pi(l_{m,n}-1)}{L}}, \tag{34}$$

where $l_{m,n}$ is random integer variable uniformly distributed in $[1, L]$. Fig. 1a and 1b show the objective function for $p = 3$ ($f(\mathbf{X})$) and $p = 0.75$ ($u(\mathbf{X})$) respectively. Observe that, due to the convergence property of BSUM framework, in both cases the objective decreases monotonically. Since for $0 < p \leq 1$ we incorporate ϵ in the objective function, the algorithms is not dealing directly with ℓ_p-norm metric, the convergence of $f(\mathbf{X})$ (ℓ_p-norm metric) is not monotonic. This fact is shown in Fig. 1c. However, in case of $0 < p \leq 1$, $f(\mathbf{X})$ mimics the monotonous decreasing behavior of the smooth approximation function. This shows the accuracy of the

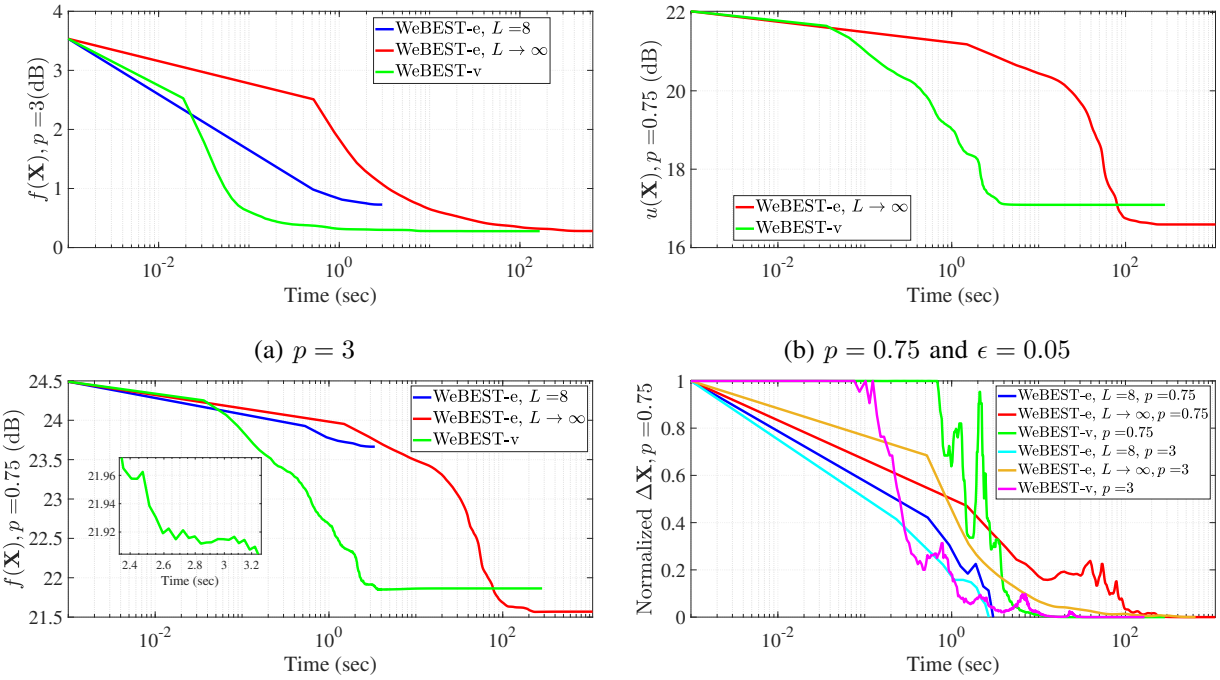

(a) $p = 3$

(b) $p = 0.75$ and $\epsilon = 0.05$

(c) ℓ_p-norm correspond to (b).

(d) Argument

Fig. 1: The convergence time of proposed method. (a) The ℓ_p-norm ($f(\mathbf{X})$) for $p = 3$, (b) the approximation function ($u(\mathbf{X})$) for $p = 0.75$, (c) the ℓ_p-norm correspond to fig (b), and (d) the argument ($\Delta\mathbf{X}^{(i)}$) ($M = 4$ and $N = 64$).

smooth approximation function. Fig. 1d shows the convergence of the argument when $p = 3$ and $p = 0.75$. In all the cases and considering the constant modulus constraint, the vector optimization offers less run-time than entry optimization.

B. ℓ_2-norm (ISL) minimization

In this part, we evaluate the performance of proposed method when $p = 2$. In this case, the proposed method minimizes the Integrated Sidelobe Level Ratio (ISLR) metric (ISLR $\triangleq \frac{\text{ISL}}{N^2}$) where the lower bound in this case is calculated by $10\log(M(M-1))$ (dB) [30]. TABLE I compares the average ISLR values of the proposed method with Multi-CAN [27], MM-Corr [30], Binary Sequences seTs (BiST) [36] and the lower bound, when $N = 64$ for different number of transmit antennas. Similar to the other methods, the proposed method meets the lower bound under continuous phase constraint. Interestingly, using the proposed method even

TABLE I: Comparison between the ISLR (dB) of the proposed method with other methods ($p = 2,\ N = 64$).

M	2	4	6	8	9	10
Initial	5.92	11.91	15.55	18.05	19.20	19.97
Lower bound	3.01	10.79	14.77	17.48	18.57	19.54
WeBEST-e, $L \to \infty$	3.01	10.79	14.77	17.48	18.57	19.54
WeBEST-v	3.01	10.79	14.77	17.48	18.57	19.54
Multi-CAN	3.01	10.79	14.77	17.48	18.57	19.54
MM-Corr	3.01	10.79	14.77	17.48	18.57	19.54
WeBEST-e, $L = 8$	3.25	10.82	14.78	17.48	18.57	19.54
BiST ($\theta = 0,\ L = 8$)	3.26	10.82	14.79	17.48	18.57	19.54

TABLE II: The ISLR obtained by the proposed method under discrete phase constraint with different length ($p = 2,\ M = 4$).

N	64	128	256	512	1024
$L = 8$	10.82	10.82	10.82	10.82	10.82

for alphabet size $L = 8$, the ISLR values of the optimized sequences are very close to the lower bound.

By keeping $M = 4$ and $L = 8$, TABLE II shows the optimized ISLR values under discrete phase constraint for different sequence lengths. Referring to the lower bound in the TABLE I, we observe that the ISLR values of the optimized sequences are very close to the lower bound.

C. ℓ_p-norm minimization for $p \geq 2$

To perform PSL minimization, we consider an increasing scheme for selection of p in several steps. Precisely, we select p_1, p_2, ..., p_T, such that $2 \leq p_1 < p_2 < \cdots < p_T < \infty$. We initialize the algorithm with a set of random sequences and design the waveform with $p = p_1$. Then we select the optimized solution of ℓ_{p_1}-norm as the initial waveform for ℓ_{p_2}-norm minimization, and so on. We repeat this procedure until we cover all of the p_i values ($i \in 1, \ldots, T$). Finally, we choose the designed waveform with $p = p_T$ as the solution for PSL minimization.

Fig. 2a shows the performance of PSL minimization of the proposed method based on aforementioned approach for $p \in \{2, 3, 4, 5, 6, 7, 8, 16, 32, 64, 128\}$. In this figure, we initialize

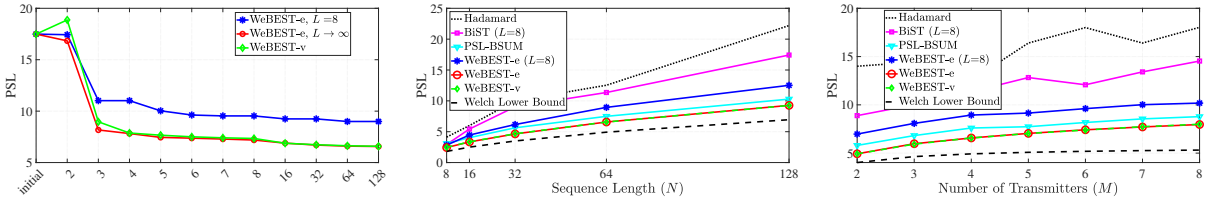

(a) PSL versus p ($M = 4$ and $N = 64$.

(b) PSL versus sequence length ($M = 4$).

(c) PSL versus number of transmitters ($N = 64$).

Fig. 2: The PSL behavior of the proposed method with the increasing scheme of value $p \in \{2, 3, 4, 5, 6, 7, 8, 16, 32, 64, 128\}$ and comparing the PSL value with PSL-BSUM, BiST and Welch lower bound.

both **Algorithm 3** and **Algorithm 1** with the same set of random MPSK sequences, with $L = 8$. It can be observed from Fig. 2a that the PSL decreases further when p increases. In Fig. 2b, we fix the number of transmit antennas ($M = 4$) and report the PSL values of the optimized sequences at different sequence lengths. Vice versa in Fig. 2c, we fix the sequence length to $N = 64$ and report the PSL values of the optimized sequences for different number of transmitters. In both figures we compare the performance of the proposed method with BiST [36] ($\theta = 1$), BSUM-PSL [39], and the available lower bound for PSL (Welch lower bound), which is given by [46], [47],

$$B_{PSL} = \sqrt{\frac{M-1}{2MN-M-1}}. \tag{35}$$

In this figure, we consider *Hadamard Code* as an initial waveform for all the algorithms. Further, for a fair comparison, we drop the spectral constraint in BSUM-PSL. It can be observed that considering the discrete phase constraint, WeBEST-e outperforms the BiST method ($L = 8$). In the case of continuous phase constraint, the performance of WeBEST-v and WeBEST-e ($L \to \infty$) are almost the same and they outperform the BSUM-PSL. Indeed, WeBEST-v and WeBEST-e ($L \to \infty$) fill the available gap between PSL values of the state-of-the-art and Welch lower bound.

D. ℓ_p-norm minimization for $0 < p \leq 1$

In this part, inverse to PSL minimization we consider a decreasing scheme for the values of p, i. e., $1 \geq p_1 > p_2 > \cdots > p_{T'} > 0$. We initialize the algorithm with a set of random sequences

and design the waveform with $p = p_1$. Then we select the optimized solution of ℓ_{p_1}-norm as the initial waveform for ℓ_{p_2}-norm minimization, and so on. We repeat this procedure until we cover all of the p_i values ($i \in 1, \ldots, T'$). Finally, we choose the designed waveform with $p = p_{T'}$ as the solution for sparse auto and cross-correlation.

To identify the sparsity, we consider a threshold for the lags of auto- and cross-correlation sidelobes. If the absolute value of the lags is less than that the threshold, we assume that the lags is zero, and count it as a sparse lag. We choose 1 as the threshold, since $|r_{m,l}(N-1)| = |x_{m,N}x^*_{l,1}| = 1$, is the lowest possible PSL value for unimodular sequences [48]. Let N_s be the number of lags of auto- and cross-correlations whose absolute value is less than 1. We define the sparsity value as,

$$S_p = \frac{N_s}{M^2(2N-1)},$$

where $S_p \in [0, 1]$, and the denominator ($M^2(2N-1)$) is the total number of lags of auto and cross-correlations. By this definition, if $S_p \to 1$ means that the auto- and cross-correlation of set of sequences are sparse, and vice versa if $S_p \to 0$ means that the auto- and cross-correlation of the set of sequences are not sparse.

Fig. 3a shows the sparsity behavior of the optimized sequences with decreasing scheme of p ($p \in \{1, 2^{-1}, 2^{-2}, 2^{-3}, 2^{-4}, 2^{-5}, 2^{-6}, 2^{-7}, \}$). As can be seen, by decreasing the value of p we obtain higher sparsity. In Fig. 3a, we fix the number of transmit antennas ($M = 4$) and report the sparsity values of the optimized sequences at different sequence lengths. Vice versa in Fig. 3c, we fix the sequence length to $N = 64$ and report the sparsity values of the optimized sequences for different number of transmitters. In these figures, we use Hadamard code as the initial set of sequences. Comparing with BiST ($\theta = 0$) [36] and Multi-CAN, Fig. 3b and Fig. 3c show a higher sparsity for the proposed method.

E. The impact of weighting

In this part, we evaluate the impact of the weight parameter ($\mathbf{w}$) on the auto- and cross-correlation sidelobes of the optimized sequences. Fig. 4 shows the impact of $\mathbf{w}$ for different values of p when $M = 2$, $N = 256$. In this figure, we consider different regions for the desired lags, precisely we set $\mathcal{V} = [-90, 90]$, $\mathcal{V} = [-64, 64]$ and $\mathcal{V} = [-38, 38]$. It can be observed from Fig. 4 that nulls are deeper if the interval of $\mathcal{V}$ is smaller.

In Fig. 5, we compare the performance of the proposed method with MM-WeCorr [30] and Multi-WeCAN [27]. In this figure, we assume that $p = 2$, $M = 2$, $N = 512$, and we consider

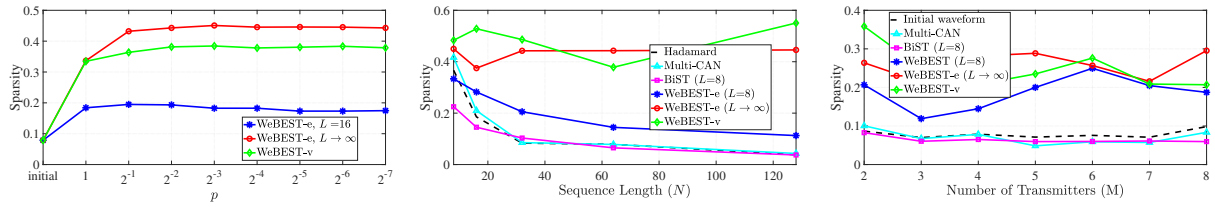

(a) Sparsity versus p ($M = 4$ and $N = 64$).

(b) Sparsity versus sequence length ($M = 4$).

(c) Sparsity versus transmitter ($N = 64$).

Fig. 3: The Sparsity behavior and comparing the performance of the proposed method with other methods.

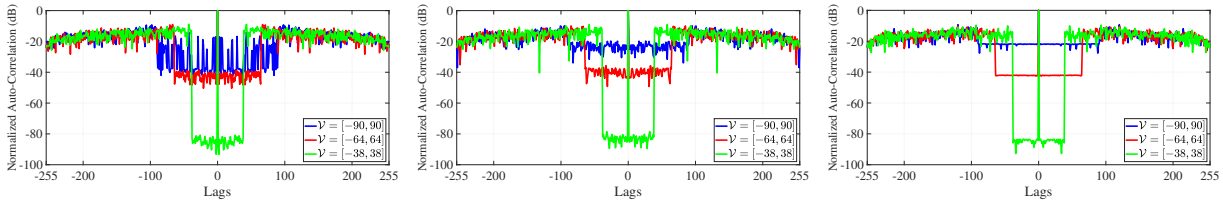

(a) $p \to 0$.

(b) $p = 2$.

(c) $p \to \infty$.

Fig. 4: The impact of weighting in WeBEST-e with different values of p ($L \to \infty$, $M = 2$ and $N = 256$).

$\mathcal{V} = [-51, 51]$. As can be seen, the proposed method outperforms the Multi-WeCAN method. Note that, the vector optimization approach has similar performance comparing to MM-WeCorr. However, the entry optimization approach offers lower sidelobes in the lag region $\mathcal{V} = [-51, 51]$ when compared to MM-WeCorr.

F. Computational Time

In this subsection, we assess the run-time of WeBEST and compare it with Multi-WeCAN and MM-WeCorr. In this regard, we report the computational time using a desktop PC with Intel (R) Core (TM) i9-9900K CPU @ 3.60GHz with installed memory (RAM) 64.00 GB. Fig. 6 shows the computational time of WeBEST, Multi-WeCAN and MM-WeCorr with $p = 2$, $M = 2$, $l = 64$ at different sequence lengths. In this figure, we assume that the desired lags are located at $\mathcal{V} = [-\lfloor 0.1N \rceil, \lfloor 0.1N \rceil]$. For fair comparison, we assume $\Delta \mathbf{X} = 10^{-3}$ as stopping threshold for all methods.

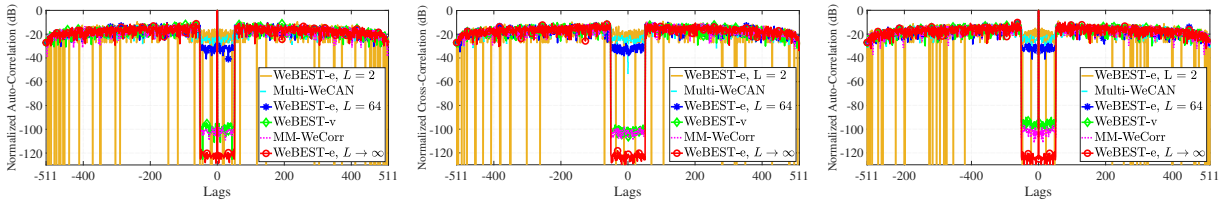

(a) The Auto-Correlation of the first waveform. (b) The Cross-Correlation of the first and second waveforms. (c) The Auto-Correlation of the second waveform.

Fig. 5: Comparison of the performance of the weighted ISL minimization of the proposed method with MM-WeCorr and Multi-WECAN unde discrete phase, entry and vector optimization ($p = 2$, $M = 2$ and $N = 512$).

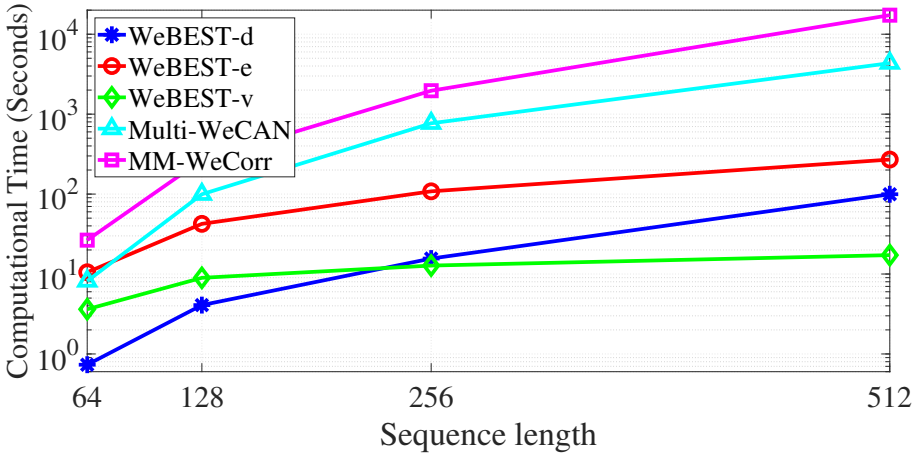

Fig. 6: Comparison of the run-time of WeBEST with other methods. ($p = 2$, $M = 2$ and $L = 64$)

V. Performance Comparison in SISO case

Fig. 7 shows the performance of WeBEST-v and GD-based method [21] in terms of PSL, for different values of p and different initial waveforms, when $M = 1$. In this figure, we consider Golomb and random phase sequences of length $N = 128$ as initial waveforms. Besides, since the GD-based method [21] just admit the even values of p, we consider an increasing scheme of p in the set $p = \{2, 4, 6, 8, 10, 12\}$ (from the lowest to the largest value of p), while for WeBEST-v, we consider the set $p = \{1, 2, 3, 4, 5, 6, 7, 8, 9, 10, 11, 12\}$. The termination threshold is $\zeta = 10^{-9}$ for both methods. It can be observed from the figure that regardless of the initial

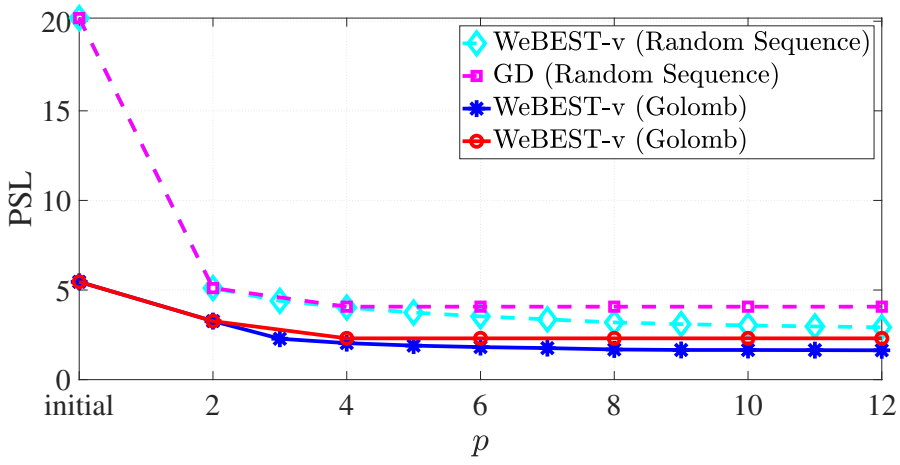

Fig. 7: The comparison of the PSL value of WeBEST-v and GD-based method with different values of p ($M = 1$, $N = 128$, $p \in \{2, 4, 6, 8, 10, 12\}$ for GD-based method [21] and $p \in \{2, 3, 4, 5, 6, 7, 8, 9, 10, 11, 12\}$ for WeBEST-v method).

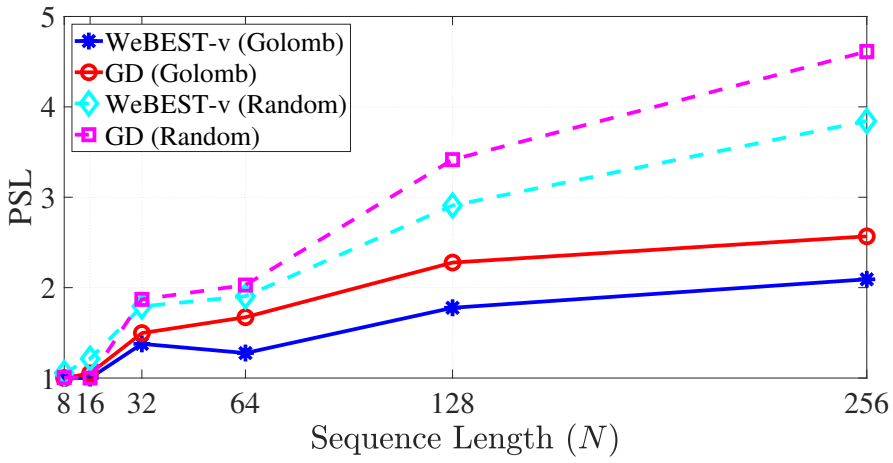

Fig. 8: The comparison of the PSL of WeBEST-v and GD-based method with different sequence length ($M = 1$).

waveform, WeBEST-v offers better PSL in comparison to GD-based method. Observe that, the GD-based method, does not solve the problem for odd values of p, while WeBEST-v solves the ℓ_p-norm problem in these points. Probably, solving the ℓ_p-norm at odd points caused to obtain a better performance in comparison with GD-based method.

TABLE III compares the convergence time of WeBEST-v and GD-based method. In this table the simulation setup is similar to Fig. 8. It can be observed from the table that the proposed

TABLE III: Convergence time (sec) of WeBEST-v and GD-based method ($M = 1$).

N	8	16	32	64	128	256
WeBEST-v (Golomb)	0.7	1.4	4.3	7.2	25	78
GD (Golomb)	212	300	204	400	559	379
WeBEST-v (Random)	1.2	1.5	3.2	7.8	62	50
GD (Random)	141	39	207	415	1020	970

method offers lower convergence time in comparison with GD-based method.

VI. Sparse auto- and cross-correlation

In this part, we show how we can design waveform with sparse auto- and cross-correlation sidelobes using the $\ell_{p\to 0}$ metric. To this end, Fig. 9 shows the range-Doppler profile for the cases when $\ell_{p\to 0}$ and ℓ_{32} was considered as the objective function for the waveform design problem under discrete phase constraint. In this figure, we assume $N = 1024$, $M = 3$, and alphabet size $L = 32$. First, we consider three targets located at $[40, 50, 60]^T$ meters distance to the radar, at the same velocity $30km/h$, angle 30^o and similar Radar Cross Section (RCS) $30m^2$. In this case, both waveforms have almost equivalent performance in terms of possibility of detecting targets. Then, we consider distributed targets are located from 50 to 55 meter distance to the radar. In this case, waveforms which are optimized using ℓ_0-norm can identify more targets. This is due to the fact that, because of sparsity in auto- and cross-correlation functions of the optimized waveforms by ℓ_0-norm, less number of targets are masked in this case in comparison to ℓ_{32}-norm.

VII. Conclusion

In this paper, we considered the ℓ_p-norm of auto- and cross-correlation functions of a set of sequences as the objective function and optimized the sequences under unimodular constraint using BSUM framework. This problem formulation, provided further the flexibility for selecting p and adapting waveforms based on the environmental conditions, a key requirement for the emerging cognitive radar systems. To tackle the problem, in every iteration of BSUM algorithm, we utilized a local approximation function to minimize the objective function. Specifically, we introduced entry- and vector-based solutions where in the former we obtain critical points and

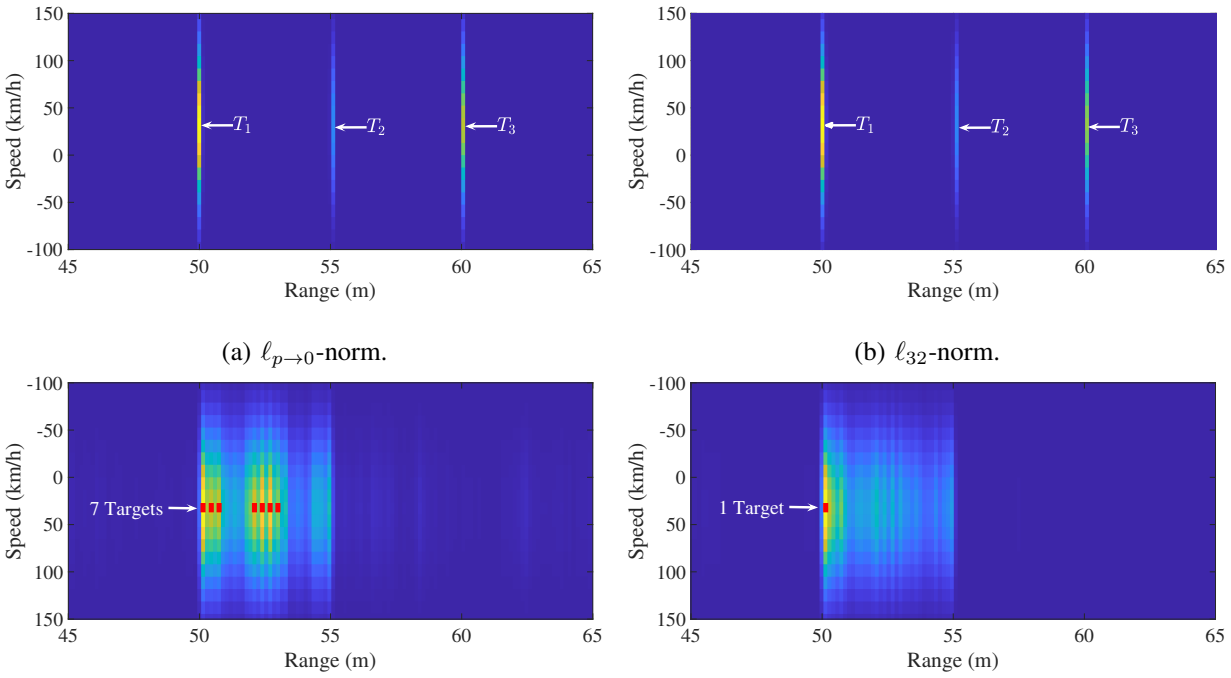

(a) $\ell_{p\to 0}$-norm.

(b) ℓ_{32}-norm.

(c) $\ell_{p\to 0}$-norm.

(d) ℓ_{32}-norm.

Fig. 9: Range-Doppler profile of $\ell_{p\to 0}$ and ℓ_{32}-norm with point and continuous targets ($M = 3$, $N = 1024$ and $L = 32$).

in the latter, we obtain the gradient to find the optimized solution. We further used FFT-based method for designing discrete phase sequences. Simulation results have illustrated the monotonicity of the proposed framework in minimizing the objective function. Besides, the proposed framework meets the lower bound in case of ISL minimization, and outperforms the counterparts in terms of PSL, ℓ_0-norm and computational time values.

VIII. Acknowledgement

This work was supported by the Luxembourg National Research Fund (FNR) CORE SPRINGER, ref C18/IS/12734677 and in part by European Research Council Advanced Grant AGNOSTIC EC/H2020/ERC2016ADG/742648/AGNOSTIC

Appendix A

The BSUM algorithm includes algorithms that successively optimize particular upper-bounds or local approximation functions of the original objectives in a block by block manner [49]–[54].

Let $\mathbf{X} \triangleq [\mathbf{x}_1^T; \ldots; \mathbf{x}_M^T] \in \mathbb{C}^{M \times N}$, where $\mathbf{x}_m, m = 1, \ldots, M$ is the transmitted signal from m^{th} transmitter. The following optimization problem,

$$\begin{cases} \min\limits_{\mathbf{x}} & f(\mathbf{x}_1, \mathbf{x}_2, \ldots, \mathbf{x}_M), \\ \text{s.t.} & \mathbf{x}_m \in \Psi_m, \ m = 1, \ldots, M. \end{cases} \tag{36}$$

can be iteratively obtained using BSUM by solving,

$$\begin{cases} \min\limits_{\mathbf{x}_m} & u_m(\mathbf{x}_m; \mathbf{x}_{-m}^{(i)}) \\ \text{s.t.} & \mathbf{x}_m \in \Psi_m, \quad m = 1, 2, \ldots, M \end{cases} \tag{37}$$

where u_m is *local approximation* of the objective function and $\mathbf{x}_{-m}^{(i)}$ represent the variable blocks that are kept fixed in the current iteration. If at some point, the objective is not decreasing at every coordinate direction, then we have obtained the optimum $\mathbf{X}^\star \equiv \mathbf{X}^{(i+1)} \triangleq [\mathbf{x}_1^{(i+1)^T}; \mathbf{x}_2^{(i+1)^T}; \ldots; \mathbf{x}_M^{(i+1)^T}]$. The above framework is rather general, and leaves us the freedom of how to choose the index m at i-th iteration (see [50], [55], [56] for more details).

The local approximation functions play an important role to simplify and efficiently solve the optimization problem. In the following, we introduce some local approximation functions which reduce the weighted ℓ_p-norm problem of (3) to simpler quadratic forms for $0 < p \leq 1$ and $p \geq 2$.

1) local approximation Function for $p \geq 2$: In this case, one choice for local approximation function is using majorization function [50]. Let $u(\mathbf{x})$ be a majorization (minorization) function of $f(\mathbf{x})$ and $\mathbf{x}^{(i)}$ be the variable at $i^{(th)}$ iteration. This function must satisfy the following conditions [57],

$$u(\mathbf{x}^{(i)}) = f(\mathbf{x}^{(i)}); \ \forall \mathbf{x}^{(i)} \in \mathcal{X} \tag{38a}$$

$$u(\mathbf{x}) \geq f(\mathbf{x}) \ (\text{minorize: } u(\mathbf{x}) \leq f(\mathbf{x})); \ \forall \mathbf{x}, \in \mathcal{X} \tag{38b}$$

$$\nabla u(\mathbf{x}^{(i)}) = \nabla f(\mathbf{x}^{(i)}); \ \forall \mathbf{x}^{(i)} \in \mathcal{X} \tag{38c}$$

$$u(\mathbf{x}) \text{ is continuous } \forall \mathbf{x}, \in \mathcal{X}. \tag{38d}$$

Lemma A.1: Let $f(x) = |x|^p$ and $|x| \in [0, \tau]$ be a real-valued function with $p \geq 2$. Then $u(x) = \eta|x|^2 + \psi|x| + \nu$ is a majorization function of $f(x)$ where, $\eta = \frac{\tau^p + (p-1)|x^{(i)}|^p - p\tau|x^{(i)}|^{p-1}}{(\tau - x^{(i)})^2}$, $\psi = p|x^{(i)}|^{p-1} - 2\eta|x^{(i)}|$ and $\nu = \eta|x^{(i)}|^2 - (p-1)|x^{(i)}|^p$.

proof A.2: See [17].

Therefore when $p \geq 2$, $|w_k r_{m,l}(k)|^p$ is majorized by (4) where,

$$\begin{aligned}
\eta_{mlk} &\triangleq \frac{\tau^p + (p-1)|w_k r_{m,l}^{(i)}(k)|^p - p\tau|w_k r_{m,l}^{(i)}(k)|^{p-1}}{(\tau - |w_k r_{m,l}^{(i)}(k)|)^2}, \\
\psi_{mlk} &\triangleq p|w_k r_{m,l}^{(i)}(k)|^{p-1} - 2\eta_{mlk}|w_k r_{m,l}^{(i)}(k)|, \\
\nu_{mlk} &\triangleq \eta_{mlk}|w_k r_{m,l}^{(i)}(k)|^2 - (p-1)|w_k r_{m,l}^{(i)}(k)|^p,
\end{aligned} \tag{39}$$

and

$$\tau \triangleq \left(\sum_{-N-1}^{N-1} |w_k r_{m,l}^{(i)}(k)|^p\right)^{\frac{1}{p}}. \tag{40}$$

2) local approximation Function for $0 < p \leq 1$*:* $f(\mathbf{X})|_{p\to 0}$ denotes the number of non-zero elements of auto- and cross-correlation.

Lemma A.3: Let $f(x) = |x|^p$ be a real-valued function with $0 < p \leq 1$. The function $f(x)$ is majorized by $\eta|x|^2 + \nu$ where, η and ν are determined by the following two conditions,

$$f(x^{(i)}) = \eta(x^{(i)})^2 + \nu, \quad f'(x^{(i)}) = 2\eta x^{(i)}$$

proof: See [42].

In this regard $|w_k r_{m,l}(k)|^p$ with $0 < p \leq 1$ is majorized with the following simpler quadratic function,

$$u(w_k r_{m,l}(k)) \triangleq \eta_{mlk}|w_k r_{m,l}(k)|^2 + \nu_{mlk}, \tag{41}$$

where, the coefficients η_{mlk} and ν_{mlk} is obtained by solving the following system of equation [42],

$$\begin{aligned}
f(w_k r_{m,l}^{(i)}(k)) =& u(w_k r_{m,l}^{(i)}(k)) \\
\frac{\partial f(w_k r_{m,l}^{(i)}(k))}{\partial |w_k r_{m,l}^{(i)}(k)|} =& 2\eta_{mlk}|w_k r_{m,l}^{(i)}(k)|,
\end{aligned} \tag{42}$$

resulting in,

$$\begin{aligned}
\nu_{mlk} &= f(w_k r_{m,l}^{(i)}(k)) - \eta_{mlk}|w_k r_{m,l}^{(i)}(k)|^2 \\
\eta_{mlk} &= \frac{\partial f(w_k r_{m,l}^{(i)}(k))}{\partial |w_k r_{m,l}^{(i)}(k)|} \times \frac{1}{2|w_k r_{m,l}^{(i)}(k)|}.
\end{aligned} \tag{43}$$

According to (43) the quadratic functions in (41), (43) are non-differentiable and singular when $w_k r_{m,l}(k) = 0$. A possible solution is to incorporate a small $\epsilon > 0$ that avoids this singularity issue and use the smooth approximation functions $f^{\epsilon}(w_k r_{m,l}(k))$ as follow [42],

$$f^{\epsilon}(w_k r_{m,l}(k)) = \begin{cases} \frac{p}{2}\epsilon^{p-2}|w_k r_{m,l}(k)|^2 & |w_k r_{m,l}(k)| \leqslant \epsilon \\ |w_k r_{m,l}(k)|^p - (1 - \frac{1}{p})\epsilon^p & |w_k r_{m,l}(k)| > \epsilon \end{cases} \tag{44}$$

Substituting (44) in (43) we have,

$$\eta_{mlk} = \begin{cases} \dfrac{p\epsilon^{(p-2)}}{2} & |w_k r_{m,l}(k)| \leqslant \epsilon \\ \dfrac{p|w_k r_{m,l}(k)|^{(p-2)}}{2} & |w_k r_{m,l}(k)| > \epsilon \end{cases} \tag{45}$$

APPENDIX B

Substituting (14) in (4) and expanding $u(w_k r_{t,t}(k,\phi))$ and $u(w_k r_{t,l}(k,\phi))$ for $0 < p \leq 1$, we have,

$$u(w_k r_{t,t}(k,\phi)) = \sum_{n=-2}^{2} \bar{v}_n e^{jn\phi}, \quad u(w_k r_{t,l}(k,\phi)) = \sum_{n=-1}^{1} \tilde{v}_n e^{jn\phi}, \tag{46}$$

where,

$\bar{v}_{-2} \triangleq \sum_{k=-N+1}^{N-1} \eta_{ttk}(a^*_{ttdk} b_{ttdk}), \quad \bar{v}_{-1} \triangleq \sum_{k=-N+1}^{N-1} \eta_{ttk}(a^*_{ttdk} c_{ttdk} + c^*_{ttdk} b_{ttdk})$

$\bar{v}_0 \triangleq \sum_{k=-N+1}^{N-1} (\eta_{ttk}(|c_{ttdk}|^2 + |a_{ttdk}|^2 + |b_{ttdk}|^2) + \nu_{ttk}),\ \bar{v}_1 \triangleq \bar{v}^*_{-1},\ \bar{v}_2 \triangleq \bar{v}^*_{-2}$

$\tilde{v}_{-1} \triangleq 2\sum_{\substack{l=1 \\ l\neq t}}^{M} \sum_{k=-N+1}^{N-1} \eta_{tlk} a^*_{tldk} c_{tldk},\ \tilde{v}_0 \triangleq 2\sum_{\substack{l=1 \\ l\neq t}}^{M} \sum_{k=-N+1}^{N-1} (\eta_{tlk}(|c_{tldk}|^2 + |a_{tldk}|^2) + \nu_{tlk}),\ \tilde{v}_1 \triangleq \tilde{v}^*_{-1},$

For $p \geq 2$, (4) is majorized by [17],

$$u(w_k r_{m,l}(k)) \triangleq \eta_{mlk} |w_k r_{m,l}(k)|^2 + \psi_{mlk} \Re\left\{ w^*_k r^*_{m,l}(k) \frac{w_k r^{(i)}_{m,l}(k)}{|w_k r^{(i)}_{m,l}(k)|} \right\} + \nu_{mlk} \tag{47}$$

Like wise, substituting (14) in (47) and expanding $u(w_k r_{t,t}(k,\phi))$ and $u(w_k r_{t,l}(k,\phi))$ for $p \geq 2$, we have,

$$u(w_k r_{t,t}(k,\phi)) = \sum_{n=-2}^{2} \bar{u}_n e^{jn\phi} + \Re\left\{ \sum_{n=-1}^{1} \hat{u}_n e^{jn\phi} \right\},$$

$$u(w_k r_{t,l}(k,\phi)) = \sum_{n=-1}^{1} \tilde{u}_n e^{jn\phi} + \Re\left\{ \sum_{n=-1}^{1} \check{u}_n e^{jn\phi} \right\},$$

Defining $\psi'_{ttk} \triangleq \frac{\psi_{ttk}}{|w_k r^{(i)}_{t,t}(k)|}$ and $\psi'_{tlk} \triangleq \frac{\psi_{tlk}}{|w_k r^{(i)}_{t,l}(k)|}$, it is shown that,

$\bar{u}_{-2} \triangleq \sum_{k=-N+1}^{N-1} \eta_{ttk} a^*_{ttdk} b_{ttdk},\ \bar{u}_{-1} \triangleq \sum_{k=-N+1}^{N-1} \eta_{ttk}(a^*_{ttdk} c_{ttdk} + c^*_{ttdk} b_{ttdk}),$

$\bar{u}_0 \triangleq \sum_{k=-N+1}^{N-1} (\eta_{ttk}(|c_{ttdk}|^2 + |a_{ttdk}|^2 + |b_{ttdk}|^2) + \nu_{ttk}),\ \bar{u}_1 \triangleq \bar{u}^*_{-1},\ \bar{u}_2 \triangleq \bar{u}^*_{-2},$

$\hat{u}_{-1} \triangleq \sum_{k=-N+1}^{N-1} \psi'_{ttk}(|c_{ttdk}|^2 + c^*_{ttdk} a_{ttdk} e^{j\phi^{(i)}} + c^*_{ttdk} b_{ttdk} e^{-j\phi^{(i)}})$

$\hat{u}_0 \triangleq \sum_{k=-N+1}^{N-1} \psi'_{ttk}(|b_{ttdk}|^2 e^{-j\phi^{(i)}} + b^*_{ttdk} a_{ttdk} e^{j\phi^{(i)}} + b^*_{ttdk} c_{ttdk})$

$\hat{u}_1 \triangleq \sum_{k=-N+1}^{N-1} \psi'_{ttk}(|a_{ttdk}|^2 e^{j\phi^{(i)}} + a^*_{ttdk} b_{ttdk} e^{-j\phi^{(i)}} + a^*_{ttdk} c_{ttdk})$

$\tilde{u}_{-1} \triangleq 2\sum_{\substack{l=1 \\ l\neq t}}^{M} \sum_{k=-N+1}^{N-1} \eta_{tlk} c_{tldk} a^*_{tldk},\ \tilde{u}_0 \triangleq 2\sum_{\substack{l=1 \\ l\neq t}}^{M} \sum_{k=-N+1}^{N-1} (\eta_{tlk}(|c_{tldk}|^2 + |a_{tldk}|^2) + \nu_{tldk})),\ \tilde{u}_1 \triangleq \tilde{u}^*_{-1}$

$\check{u}_{-1} \triangleq 2\sum_{\substack{l=1 \\ l\neq t}}^{M} \sum_{k=-N+1}^{N-1} \psi'_{tlk}(|c_{tldk}|^2 + c^*_{tldk} a_{tldk} e^{j\phi^{(i)}}),\ \check{u}_0 \triangleq 2\sum_{\substack{l=1 \\ l\neq t}}^{M} \sum_{k=-N+1}^{N-1} \psi'_{tlk}(|c_{tldk}|^2 + c^*_{tldk} a_{tldk} e^{j\phi^{(i)}})$

$\breve{u}_1 \triangleq 2\sum_{\substack{l=1\\l\neq t}}^{M}\sum_{k=-N+1}^{N-1}\psi'_{tlk}(|a_{tldk}|^2 e^{j\phi^{(i)}} + a^*_{tldk}c_{tldk})$

In this regard, readily it is shown that the problem (15) is written as (16), where the coefficients are,

$$v_{n;\in\{-2,2\}} \triangleq \begin{cases} \bar{v}_n & 0 < p \leq 1 \\ \bar{u}_n & p \geq 2 \end{cases}, \quad v_{n;\in\{-1,0,1\}} \triangleq \begin{cases} \bar{v}_n + \tilde{v}_n & 0 < p \leq 1 \\ \bar{u}_n + \tilde{u}_n + \hat{u}_n + \breve{u}_n & p \geq 2 \end{cases} \tag{48}$$

APPENDIX C

Substituting $e^{jn\phi} = \cos(n\phi) + j\sin(n\phi)$ in $u'(\phi)$ and separating the real and imaginary part, $u'(\phi)$ becomes,

$$u'(\phi) = \xi_0\cos^2(\phi) + \xi_1\sin^2(\phi) + \xi_2\sin(\phi)\cos(\phi) + \xi_3\cos(\phi) + \xi_4\sin(\phi) \tag{49}$$

where, $\xi_0 \triangleq 2\Im\{v_{-2} - v_2\}$, $\xi_1 \triangleq 2\Im\{v_2 - v_{-2}\}$, $\xi_2 \triangleq -4\Re\{v_2 + v_{-2}\}$, $\xi_3 \triangleq \Im\{v_{-1} - v_1\}$ and $\xi_4 \triangleq -\Re\{v_{-1} + v_1\}$. Using the change variable $z \triangleq \tan(\frac{\phi}{2})$ and substituting $\cos(\phi) = (1-z^2)/(1+z^2)$, $\sin(\phi) = 2z/(1+z^2)$ in $u'(\phi)$, it is written as, $u'(z) = \frac{\sum_{k=0}^{4} s_k z^k}{(1+z^2)^2}$, where,

$$s_0 \triangleq \xi_0 + \xi_3,\ \ s_1 \triangleq 2(\xi_2 + \xi_4),\ \ s_2 \triangleq 2(2\xi_1 - \xi_0), s_3 \triangleq 2(\xi_4 - \xi_2),\ \ s_4 \triangleq \xi_0 - \xi_3 \tag{50}$$

APPENDIX D

Let assume that $l' = \{1, 2, \ldots, L\}$ be the indices of alphabet Ω_L. Therefore the objective function is written as,

$$\begin{aligned} f(l') = f(\mathbf{X}_{-t}) + 2\sum_{\substack{l=1\\l\neq t}}^{M}\sum_{k=-N+1}^{N-1}|a_{tldk} + c_{tldk}e^{-j2\pi\frac{l'-1}{L}}|^p \\ + \sum_{k=-N+1}^{N-1}|a_{ttdk} + c_{ttdk}e^{-j2\pi\frac{l'-1}{L}} + b_{ttdk}e^{-j4\pi\frac{l'-1}{L}}|^p \end{aligned} \tag{51}$$

Let assume that $\mathbf{y} \in \mathbb{C}^N$ be a vector and $\mathcal{F}_L\{\mathbf{y}\} \triangleq \sum_{n=1}^{N} y(n)e^{j2\pi\frac{(n-1)(l'-1)}{L}}$ be the L point DFT operator of $\mathbf{y}$. Therefore, it can be shown that all the possible values of $a_{tldk} + c_{tldk}e^{-j2\pi\frac{l'-1}{L}}$ and $a_{ttdk} + c_{ttdk}e^{-j2\pi\frac{l'-1}{L}} + b_{ttdk}e^{-j4\pi\frac{l'-1}{L}}$ for $l' = \{1, 2, \ldots, L\}$, are obtained by $\mathcal{F}_L\{a_{tldk}, c_{tldk}\}$ and $\mathcal{F}_L\{a_{ttdk}, c_{ttdk}, b_{ttdk}\}$ respectively. Therefore, the optimum index is obtained as (22).

REFERENCES

[1] S. D. Blunt and E. L. Mokole, "Overview of radar waveform diversity," *IEEE Aerospace and Electronic Systems Magazine*, vol. 31, no. 11, pp. 2–42, 2016.

[2] M. Kumar and V. Chandrasekar, "Intrapulse polyphase coding system for second trip suppression in a weather radar," *IEEE Transactions on Geoscience and Remote Sensing*, vol. 58, no. 6, pp. 3841–3853, 2020.

[3] J. M. Baden, "Efficient optimization of the merit factor of long binary sequences," *IEEE Trans. Inf. Theory*, vol. 57, no. 12, pp. 8084–8094, Dec 2011.

[4] H. Sun, F. Brigui, and M. Lesturgie, "Analysis and comparison of MIMO radar waveforms," in *2014 International Radar Conference*, Oct 2014, pp. 1–6.

[5] "Texas instrument: MIMO radar, application report, swra554," https://www.ti.com/lit/an/swra554a/swra554a.pdf, accessed: 2021-03-15.

[6] C. Hammes, B. S. M. R., and B. Ottersten, "Generalized multiplexed waveform design framework for cost-optimized MIMO radar," *IEEE Trans. Signal Process.*, vol. 69, pp. 88–102, 2021.

[7] "Ultra-small, economical and cheap radar made possible thanks to chip technology," https://www.imec-int.com/en/imec-magazine/imec-magazine-march-2018/ultra-small-economical-and-cheap-radar-made-possible-thanks-to-chip-technology, accessed: 2021-03-15.

[8] E. Raei, S. Sedighi, M. Alaee-Kerahroodi, and M. B. Shankar, "MIMO radar transmit beampattern shaping for spectrally dense environments," *IEEE Transactions on Aerospace and Electronic Systems*, pp. 1–13, 2022.

[9] M. Alaee-Kerahroodi, E. Raei, S. Kumar, and B. S. M. R. R., "Cognitive radar waveform design and prototype for coexistence with communications," *IEEE Sensors Journal*, vol. 22, no. 10, pp. 9787–9802, 2022.

[10] J. R. Guerci, R. M. Guerci, M. Ranagaswamy, J. S. Bergin, and M. C. Wicks, "CoFAR: Cognitive fully adaptive radar," in *2014 IEEE Radar Conference*, 2014, pp. 0984–0989.

[11] P. Stinco, M. Greco, F. Gini, and B. Himed, "Cognitive radars in spectrally dense environments," *IEEE Aerospace and Electronic Systems Magazine*, vol. 31, no. 10, pp. 20–27, 2016.

[12] S. Z. Gurbuz, H. D. Griffiths, A. Charlish, M. Rangaswamy, M. S. Greco, and K. Bell, "An overview of cognitive radar: Past, present, and future," *IEEE Aerospace and Electronic Systems Magazine*, vol. 34, no. 12, pp. 6–18, 2019.

[13] A. De Maio and A. Farina, "The role of cognition in radar sensing," in *2020 IEEE Radar Conference (RadarConf20)*, 2020, pp. 1–6.

[14] P. Stoica, H. He, and J. Li, "New algorithms for designing unimodular sequences with good correlation properties," *IEEE Trans. Signal Process.*, vol. 57, no. 4, pp. 1415–1425, Apr 2009.

[15] P. Stoica, H. He, and J. Li, "On designing sequences with impulse-like periodic correlation," *IEEE Signal Processing Letters*, vol. 16, no. 8, pp. 703–706, 2009.

[16] J. Song, P. Babu, and D. Palomar, "Optimization methods for designing sequences with low autocorrelation sidelobes," *IEEE Trans. Signal Process.*, vol. 63, no. 15, pp. 3998–4009, Aug 2015.

[17] J. Song, P. Babu, and D. P. Palomar, "Sequence design to minimize the weighted integrated and peak sidelobe levels," *IEEE Trans. Signal Process.*, vol. 64, no. 8, pp. 2051–2064, Apr 2016.

[18] L. Zhao, J. Song, P. Babu, and D. P. Palomar, "A unified framework for low autocorrelation sequence design via Majorization-Minimization," *IEEE Trans. Signal Process.*, vol. 65, no. 2, pp. 438–453, Jan 2017.

[19] J. Liang, H. C. So, J. Li, and A. Farina, "Unimodular sequence design based on alternating direction method of multipliers," *IEEE Trans. Signal Process.*, vol. 64, no. 20, pp. 5367–5381, 2016.

[20] M. Alaee-Kerahroodi, A. Aubry, A. De Maio, M. M. Naghsh, and M. Modarres-Hashemi, "A coordinate-descent framework to design low PSL/ISL sequences," *IEEE Trans. Signal Process.*, vol. 65, no. 22, pp. 5942–5956, Nov 2017.

[21] J. M. Baden, B. O'Donnell, and L. Schmieder, "Multiobjective sequence design via gradient descent methods," *IEEE Trans. Aerosp. Electron. Syst.*, vol. 54, no. 3, pp. 1237–1252, June 2018.

[22] R. Lin, M. Soltanalian, B. Tang, and J. Li, "Efficient design of binary sequences with low autocorrelation sidelobes," *IEEE Trans. Signal Process.*, vol. 67, no. 24, pp. 6397–6410, Dec 2019.

[23] Y. Bu, X. Yu, J. Yang, T. Fan, and G. Cui, "A new approach for design of constant modulus discrete phase radar waveform with low WISL," *Signal Processing*, vol. 187, p. 108145, 2021. [Online]. Available: https://www.sciencedirect.com/science/article/pii/S0165168421001833

[24] S. P. Sankuru and P. Babu, "A fast iterative algorithm to design phase-only sequences by minimizing the isl metric," *Digital Signal Processing*, vol. 111, p. 102991, 2021. [Online]. Available: https://www.sciencedirect.com/science/article/pii/S1051200421000300

[25] W. Fan, J. Liang, G. Yu, H. C. So, and G. Lu, "Minimum local peak sidelobe level waveform design with correlation and/or spectral constraints," *Signal Processing*, vol. 171, p. 107450, 2020. [Online]. Available: https://www.sciencedirect.com/science/article/pii/S0165168419305018

[26] W. Fan, J. Liang, H. C. So, and G. Lu, "Min-max metric for spectrally compatible waveform design via log-exponential smoothing," *IEEE Transactions on Signal Processing*, vol. 68, pp. 1075–1090, 2020.

[27] H. He, P. Stoica, and J. Li, "Designing unimodular sequence sets with good correlations; including an application to MIMO radar," *IEEE Trans. Signal Process.*, vol. 57, no. 11, pp. 4391–4405, Nov 2009.

[28] G. Cui, X. Yu, M. Piezzo, and L. Kong, "Constant modulus sequence set design with good correlation properties," *Signal Processing*, vol. 139, pp. 75–85, 2017.

[29] Y. Li and S. A. Vorobyov, "Fast algorithms for designing unimodular waveform(s) with good correlation properties," *IEEE Trans. Signal Process.*, vol. 66, no. 5, pp. 1197–1212, March 2018.

[30] J. Song, P. Babu, and D. P. Palomar, "Sequence set design with good correlation properties via majorization-minimization," *IEEE Trans. Signal Process.*, vol. 64, no. 11, pp. 2866–2879, June 2016.

[31] M. Alaee-Kerahroodi, M. R. Bhavani Shankar, K. V. Mishra, and B. Ottersten, "Meeting the lower bound on designing set of unimodular sequences with small aperiodic/periodic ISL," in *2019 20th International Radar Symposium (IRS)*, 2019, pp. 1–13.

[32] E. Raei, M. Alaee-Kerahroodi, and M. B. Shankar, "Spatial- and range- ISLR trade-off in MIMO radar via waveform correlation optimization," *IEEE Transactions on Signal Processing*, vol. 69, pp. 3283–3298, 2021.

[33] G. Jin, A. Aubry, A. De Maio, R. Wang, and W. Wang, "Quasi-orthogonal waveforms for ambiguity suppression in spaceborne quad-pol sar," *IEEE Transactions on Geoscience and Remote Sensing*, pp. 1–17, 2021.

[34] E. Raei, M. Alaee-Kerahroodi, and B. M. R. Shankar, "Waveform design for beampattern shaping in 4d-imaging mimo radar systems," in *2021 21st International Radar Symposium (IRS)*, 2021, pp. 1–10.

[35] E. Raei, M. Alaee-Kerahroodi, and B. S. M. R. Rao, "Waveform design for range-isl minimization with spectral compatibility in MIMO radars," in *2022 19th European Radar Conference (EuRAD)*, 2022, pp. 101–104.

[36] M. Alaee-Kerahroodi, M. Modarres-Hashemi, and M. M. Naghsh, "Designing sets of binary sequences for MIMO radar systems," *IEEE Trans. Signal Process.*, pp. 1–1, 2019.

[37] S. P. Sankuru, R. Jyothi, P. Babu, and M. Alaee-Kerahroodi, "Designing sequence set with minimal peak side-lobe level for applications in high resolution radar imaging," *IEEE Open Journal of Signal Processing*, vol. 2, pp. 17–32, 2021.

[38] R. Lin and J. Li, "On binary sequence set design with applications to automotive radar," in *ICASSP 2020 - 2020 IEEE International Conference on Acoustics, Speech and Signal Processing (ICASSP)*, 2020, pp. 8639–8643.

[39] W. Fan, J. Liang, Z. Chen, and H. C. So, "Spectrally compatible aperiodic sequence set design with low cross- and auto-correlation psl," *Signal Processing*, vol. 183, p. 107960, 2021. [Online]. Available: https://www.sciencedirect.com/science/article/pii/S0165168420305041

[40] H. Esmaeili-Najafabadi, M. Ataei, and M. F. Sabahi, "Designing sequence with minimum PSL using chebyshev distance and its application for chaotic MIMO radar waveform design," *IEEE Trans. Signal Process.*, vol. 65, no. 3, pp. 690–704, Feb 2017.

[41] S. Boyd and L. Vandenberghe, *Convex optimization*. Cambridge university press, 2004.

[42] J. Song, P. Babu, and D. P. Palomar, "Sparse generalized eigenvalue problem via smooth optimization," *IEEE Trans. Signal Process.*, vol. 63, no. 7, pp. 1627–1642, 2015.

[43] R. Seidel and M. Sharir, "Top-down analysis of path compression," *SIAM Journal on Computing*, vol. 34, no. 3, pp. 515–525, 2005. [Online]. Available: https://doi.org/10.1137/S0097539703439088

[44] M. R. B. Shankar and K. V. S. Hari, "Reduced complexity equalization schemes for zero padded ofdm systems," *IEEE Signal Processing Letters*, vol. 11, no. 9, pp. 752–755, 2004.

[45] G. H. Golub and C. F. Van Loan, *Matrix Computations*, 3rd ed. The Johns Hopkins University Press, 1996.

[46] L. Welch, "Lower bounds on the maximum cross correlation of signals (corresp.)," *IEEE Trans. Inf. Theory*, vol. 20, no. 3, pp. 397–399, May 1974.

[47] H. He, J. Li, and P. Stoica, *Waveform Design for Active Sensing Systems*. Cambridge University Press, 2012.

[48] K. Mohammad, Alaee, A. Augusto, N. Mohammad, Mahdi, M. Antonio, De, and H. Mahmoud, Modarres, *Radar Waveform Design Based on Optimization Theory*. Institution of Engineering and Technology, 2020, ch. A computational design of phase-only (possibly binary) sequences for radar systems, pp. 63–92.

[49] F. Laforest, "Generic models: a new approach for information systems design," in *Proceedings of the Third Basque International Workshop on Information Technology - BIWIT'97 - Data Management Systems*, 1997, pp. 189–196.

[50] M. Hong, M. Razaviyayn, Z. Luo, and J. Pang, "A unified algorithmic framework for block-structured optimization involving big data: With applications in machine learning and signal processing," *IEEE Signal Processing Magazine*, vol. 33, no. 1, pp. 57–77, 2016.

[51] P. Borwein and R. Ferguson, "Polyphase sequences with low autocorrelation," *IEEE Trans. Inf. Theory*, vol. 51, no. 4, pp. 1564–1567, Apr 2005.

[52] W. Huang, M. M. Naghsh, R. Lin, and J. Li, "Doppler sensitive discrete-phase sequence set design for MIMOs radar," *IEEE Trans. Aerosp. Electron. Syst.*, pp. 1–1, 2020.

[53] E. Raei, M. Alaee-Kerahroodi, P. Babu, and B. S. M. R, "ℓ_p-norm minimization of auto and cross correlation sidelobes in MIMO radars," in *2022 23rd International Radar Symposium (IRS)*, 2022, pp. 92–97.

[54] E. Raei, M. Alaee-Kerahroodi, and B. S. M. R., "MIMO radar transmit beampattern matching based on block successive upper-bound minimization," in *2022 30th European Signal Processing Conference (EUSIPCO)*, 2022, pp. 1901–1905.

[55] A. Aubry, A. De Maio, A. Zappone, M. Razaviyayn, and Z. Luo, "A new sequential optimization procedure and its applications to resource allocation for wireless systems," *IEEE Trans. Signal Process.*, vol. 66, no. 24, pp. 6518–6533, 2018.

[56] J. Yang, A. Aubry, A. De Maio, X. Yu, G. Cui, and S. Iommelli, "Constant modulus discrete phase radar waveforms design subject to multi-spectral constraints," in *2020 IEEE 7th International Workshop on Metrology for AeroSpace (MetroAeroSpace)*, 2020, pp. 28–31.

[57] L. Zhao and D. P. Palomar, "Maximin joint optimization of transmitting code and receiving filter in radar and communications," *IEEE Trans. Signal Process.*, vol. 65, no. 4, pp. 850–863, Feb 2017.